Studies on tissue plasminogen activator: efficiency of thrombolysis in the presence of iodinated contrast media and development of a novel targeted t-PA delivery system

PhD thesis

Author: Eszter Voros

Head of the Doctoral School: Prof. Dr. Kovacs L. Gabor M.D., Sc.D.

Head of the Doctoral Program: Prof. Kalman Toth M.D., Ph.D., Sc.D.

Supervisors: Istvan Battyani M.D., Ph.D., and

Prof. Kalman Toth M.D., Ph.D., Sc.D.

University of Pecs, Medical School, Hungary

Radiology Department, Pecs, Hungary

First Department of Medicine, Pecs, Hungary

Pecs, 2017

CONTENTS

1. Acknowledgment

Foremost, I would like to express my sincere gratitude to my advisors Prof. Istvan Battyani and Kalman Toth for their continuous support of my Ph.D. study and research, for their patience, motivation, enthusiasm, and immense knowledge. Their guidance helped me in all the time of research and writing of this thesis. I could not have imagined having a better advisors and mentors for my Ph.D study.

My sincere thanks also go to Dr. Laszlo Deres for leading me working on diverse exciting projects. I thank my fellow lab mates at the Szentagothai Research Center: Krisztian Eros, Adam Riba and Timea Dozsa.

None of these could have happened without my family, they were there for me with their own brand of humor and support over the last several years. Every time when I was ready to quit, you did not let me and I am forever grateful.

Last but not the least, I must express my very profound gratitude to my parents and to Dr. Giacomo Bruno for providing me with unfailing support and continuous encouragement throughout my years of study and through the process of researching and writing this thesis. This accomplishment would not have been possible without you. Thank you.

Eszter Voros

2. Abstract

In Western world the obstruction of critical blood vessels due to thrombosis is the leading cause of death: acute ischemic stroke, deep vein thrombosis (DVT), pulmonary embolism (PE), and acute ischemic stroke (AIS) are the major causes of cardiovascular mortality, which results in over 1 million deaths each year in the US [2,3]. Thrombosis is responsible for most of the pathophysiology of these diseases. Thrombolytic drug therapy can reduce mortality, and this therapeutic approach has been widely used in thrombosis treatment [4]. Although a number of thrombolytic drugs are currently available, tissue plasminogen activator (t-PA) is currently the only US Food and Drug Administration-approved therapy for lysis of fibrin clot in treating ischemic stroke [5].

t-PA is a serine protease that converts the zymogen plasminogen to plasmin, which initiates the process of lysis of the fibrin clot (fibrinolysis) [6]. As t-PA has a very short life in plasma (half-life ≈5 minutes) [7], it needs to be administered at a high dose for a prolonged period of time in order to maintain an effective drug level during thrombolytic drug therapy, which leads to degradation of clotting factors and hemorrhage [8]. It will therefore be highly desirable to deliver t-PA under guidance for targeted thrombolysis, which will allow t-PA to be localized to the target site and reduce its hemorrhagic side effects [9].

The major treatment strategy for DVT, PE, heart attack, and AIS is pharmacological reperfusion using intravenous t-PA. In some cases, multimodal computed tomography (CT) is performed prior to t-PA administration. While this multimodal approach provides greater information than non-contrast CT alone, radiographic contrast agents may interfere with thrombolytic therapy. The relationship between the dosage of iodinated contrast media and the efficiency of the fibrinolysis via rt-PAis poorly understood in patients receiving intravenous tissue-type plasminogen activator. Thus, in this study, we compare the effect of five different contrast media such as Xenetix®

(iobitridol), Ultravist® (iopromide), Omnipaque® (iohexol), Visipaque® (iodixanol) and Iomeron® (iomeprol) on fibrinolysis via t-PA.

Magnetic nanoparticles (MNPs) offer several advantages when used as a drug carrier, including the large surface area, which can be properly modified to attach with drug molecules. Ensuring biocompatibility and non-toxicity, iron oxide based particles (magnetite) with superparamagnetic characteristics are commonly used as the magnetically responsive component, which can be manipulated by an external magnetic field gradient. Based on these properties, the superparamagnetic nanoparticles could be transported through the vascular system, concentrated in a specific part of the body with the aid of a magnetic field, and used as a carrier for t-PA delivery. For drug delivery applications, iron oxide MNP must be pre-coated with substances that assure their stability, biodegradability, and non-toxicity in the physiological medium to achieve combined properties of high magnetic saturation, biocompatibility and interactive functions on the surface.

In this study, t-PA immobilized on the surface of bovine serum albumin (BSA) coated superparamagnetic nanoparticles. This thrombolytic nano-agent (t-PA–NCs) has demonstrated three orders of magnitude higher dissolution efficiency as compared to free t-PA and is capable of recanalizing occluded vessels in animal models with sever thrombosis. Also, their favorable toxicity profiles make t-PA–NCs a promising platform for the application of nanomedicine in thrombolytic diseases.

3. Aims of the thesis

1. Developing a reliable method to make ex vivo blot clots freshly drawn mouse or rat whole blood. Inducing thrombolysis using t-PA in known concentration and follow the progress of clot lysis over time via spectrometry by measuring the amount of released hemoglobin.
2. Testing the effect on thrombolysis therapy induced by t-PA of five different contrast media such as Xenetix® (iobitridol), Ultravist® (iopromide), Omnipaque® (iohexol), Visipaque® (iodixanol) and Iomeron® (iomeprol) using the developed ex vivo blood clot lysis model.
3. Developing and optimizing a nanocarrier platform which is suitable for targeted delivery of t-PA and other potential thrombolytic drugs using iron oxide core. Developing an alternative protocol for synthetizing labeled nanoparticles to follow up the thrombus lysis at in vitro and in vivo environment
4. Performing the sufficient physical-chemical characterizations such as measuring size, shape, Zeta-potential, stability, calculating the loaded amount of drug into the particles
5. Testing the NPs in in vitro environment with and without flow. Developing a method for making identical thrombus (mouse, pig, human) in ex vivo environment
6. Introducing the NPs into an alternative magnetic field for testing their behavior, measuring the lysis efficiency and time with heating effect
7. Developing a mouse and pig ferric chloride arterial injury model and testing the NPs in in vivo environment using intravital microscopy technique. Performing the remote guidance of NPs via external magnetic fields.

4. Introduction

Radiographic iodinated contrast media

Since their introduction in the 1950s, organic radiographic iodinated contrast media (ICM) have been among the most commonly prescribed drugs in the history of modern medicine. The phenomenon of present-day radiologic imaging would be lacking without these agents. ICM generally have a good safety record. Adverse effects from the intravascular administration of ICM are generally mild and self-limited; reactions that occur from the extravascular use of ICM are rare [10]. Nonetheless, severe or life-threatening reactions can occur with either route of administration [11-13].

Detecting sensitivity to contrast media

Brockow et al performed a prospective study to determine the specificity and sensitivity of skin tests in patients who have experienced contrast-related reactions and found that skin test specificity was 96-100%. Skin prick, intradermal, and patch tests were conducted in 220 patients with either immediate or nonimmediate reaction. For immediate reactors, the intradermal tests were the most sensitive, whereas delayed intradermal tests in combination with patch tests were needed for optimal sensitivity in nonimmediate reactors. Contrast medium cross-reactivity was more common in the nonimmediate than in the immediate group. The data suggested that at least 50% of hypersensitivity reactions to contrast media are caused by an immunologic mechanism. Skin testing appears to be a useful tool for diagnosis of contrast medium allergy and may play an important role in selection of a safe product in previous reactors [14]. In a retrospective study of 37 patients with suspected immediate hypersensitivity reaction to iodinated contrast media (ICM), the negative predictive value for skin tests and intravenous provocation test (IPT) with low dose ICM was 80% (95% CI 44-97%) [15].

Types of Iodinated Contrast Media

All currently used ICM are chemical modifications of a 2,4,6-tri-iodinated benzene ring [10] (**Figure 1**). They are classified based on their physical and chemical characteristics, including their chemical structure, osmolality, iodine content, and ionization in solution. In clinical practice, categorization based on osmolality is widely used. Osmotic effects of contrast media that are specific for the kidney include transient decreases in blood flow, filtration fraction, and glomerular filtration rate. Secondary effects include osmotically induced diuresis with a dehydrating effect [16,17].

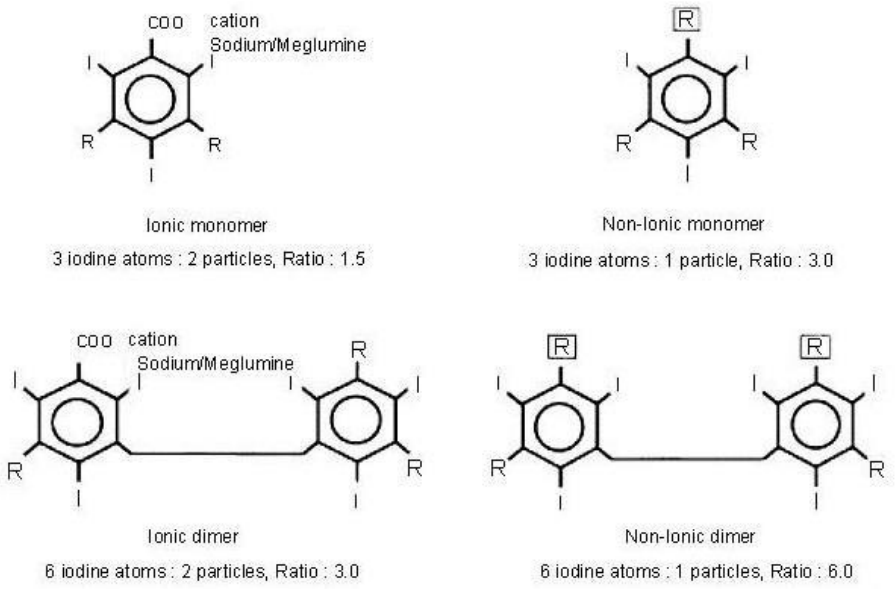

Figure 1: Chemical modifications of a 2,4,6-tri-iodinated benzene ring

High-osmolality contrast media

High-osmolality contrast media consist of a tri-iodinated benzene ring with 2 organic side chains and a carboxyl group. The iodinated anion, diatrizoate or iothalamate, is conjugated with a cation, sodium or meglumine; the result is an ionic monomer (**Figure 1**). The ionization at the carboxyl-cation bond makes the agent water soluble. Thus, for every 3 iodine atoms, 2 particles are present

in solution (ie, a ratio of 3:2). The osmolality in solution ranges from 600 to 2100 mOsm/kg, versus 290 mOsm/kg for human plasma. The osmolality is related to some of the adverse events of these contrast media. Ionic monomers are subclassified by the percentage weight of the contrast agent molecule in solution (eg, 30% or 76%). In the United States, commonly used high-osmolality ICM are Renografin (diatrizoate anion; Bracco Diagnostics Inc, Princeton, NJ) or Hypaque (diatrizoate anion; GE Healthcare, Inc, Princeton, NJ) and Conray (iothalamate anion; tyco Healthcare and Mallinckrodt Inc, St. Louis, Mo).

Low-osmolality contrast media:

There are 3 types of low-osmolality ICM: (1) nonionic monomers, (2) ionic dimers, and (3) nonionic dimers.

- **Nonionic monomers**: In nonionic monomers, the tri-iodinated benzene ring is made water soluble by the addition of hydrophilic hydroxyl groups to organic side chains that are placed at the 1, 3, and 5 positions. Lacking a carboxyl group, nonionic monomers do not ionize in solution. Thus, for every 3 iodine atoms, only 1 particle is present in solution (ie, a ratio of 3:1). Therefore, at a given iodine concentration, nonionic monomers have approximately one half the osmolality of ionic monomers in solution. At normally used concentrations, 25-76%, nonionic monomers have 290-860 mOsm/kg. Nonionic monomers are subclassified according to the number of milligrams of iodine in 1 mL of solution (eg, 240, 300, or 370 mg I/mL). The larger side chains increase the viscosity of nonionic monomers compared with ionic monomers. The increased viscosity makes nonionic monomers harder to inject, but it does not appear to be related to the frequency of adverse events. Common nonionic monomers are iohexol (Omnipaque; GE Healthcare, Inc), iopamidol (Isovue; Bracco Diagnostics Inc), ioversol (Optiray; tyco Healthcare and

Mallinckrodt Inc), and iopromide (Ultravist; Bayer HealthCare Pharmaceuticals Inc, Wayne, NJ). The nonionic monomers are the contrast agents of choice. In addition to their nonionic nature and lower osmolalities, they are potentially less chemotoxic than the ionic monomers.

- **Ionic dimers**: Ionic dimers are formed by joining 2 ionic monomers and eliminating 1 carboxyl group. These agents contain 6 iodine atoms for every 2 particles in solution (ie, a ratio of 6:2). The only commercially available ionic dimer is ioxaglate (Hexabrix; tyco Healthcare and Mallinckrodt Inc). Ioxaglate has a concentration of 59%, or 320 mg I/mL, and an osmolality of 600 mOsm/kg. Because of its high viscosity, ioxaglate is not manufactured at higher concentrations. Ioxaglate is used primarily for peripheral arteriography.
- **Nonionic dimers** Nonionic dimers consist of 2 joined nonionic monomers. These substances contain 6 iodine atoms for every 1 particle in solution (ie, ratio of 6:1). For a given iodine concentration, the nonionic dimers have the lowest osmolality of all the contrast agents. At approximately 60% concentration by weight, these agents are iso-osmolar with plasma. They are also highly viscous and, thus, have limited clinical usefulness. Examples of nonionic dimers are iotrol and iodixanol (Visipaque; Amersham Health Inc, Princeton, NJ).

Adverse reactions to iodinated contrast media

Adverse reactions to ICM are classified as idiosyncratic and non-idiosyncratic [10,18-23]. The pathogenesis of such adverse reactions probably involves direct cellular effects; enzyme induction; and activation of the complement, fibrinolytic, and other systems.

Idiosyncratic reactions

Idiosyncratic reactions typically begin within 20 minutes of the ICM injection, independent of the dose that is administered. A severe idiosyncratic reaction can occur after an injection of less than 1 mL of a contrast agent. Although reactions to ICM have the same manifestations as anaphylactic reactions, these are not true hypersensitivity reactions. [27, 28] Immunoglobulin E (IgE) antibodies are not involved. In addition, previous sensitization is not required, nor do these reactions consistently recur in each patient. For these reasons, idiosyncratic reactions to ICM are called anaphylactic reactions. The symptoms of anaphylactic reaction can be classified as mild, moderate, and severe.

Mild symptoms

Mild symptoms include the following: scattered urticaria, which is the most commonly reported adverse reaction; pruritus; rhinorrhea; nausea, brief retching, and/or vomiting; diaphoresis; coughing; and dizziness. Patients with mild symptoms should be observed for the progression or evolution of a more severe reaction, which requires treatment.

Moderate symptoms

Moderate symptoms include the following: persistent vomiting; diffuse urticaria; headache; facial edema; laryngeal edema; mild bronchospasm or dyspnea; palpitations, tachycardia, or bradycardia; hypertension; and abdominal cramps.

Severe symptoms

Severe symptoms include the following: life-threatening arrhythmias (ie, ventricular tachycardia), hypotension, overt bronchospasm, laryngeal edema, pulmonary edema, seizures, syncope, and death.

Cardiovascular reactions

ICM can cause hypotension and bradycardia. Vasovagal reactions, a direct negative inotropic effect on the myocardium, and peripheral vasodilatation probably contribute to these effects. The latter 2 effects may represent the actions of cardioactive and vasoactive substances that are released after the anaphylactic reaction to the ICM. This effect is generally self-limiting, but it can also be an indicator of a more severe, evolving reaction. ICM can lower the ventricular arrhythmia threshold and precipitate cardiac arrhythmias and cardiac arrest. Fluid shifts due to an infusion of hyperosmolar intravascular fluid can produce an intravascular hypervolemic state, systemic hypertension, and pulmonary edema. Also, ICM can precipitate angina. The similarity of the cardiovascular and anaphylactic reactions to ICM can create confusion in identifying the true nature of the type and severity of an adverse reaction; this confusion can lead to the overtreatment or undertreatment of symptoms. Other non-idiosyncratic reactions include syncope; seizures; and the aggravation of underlying diseases, including pheochromocytomas, sickle cell anemia, hyperthyroidism, and myasthenia gravis.

Radiologists and other physicians must be aware of the risk factors for reactions to contrast media, use strategies to minimize adverse events, and be prepared to promptly recognize and manage any reactions to the contrast media [18,24-27]. These signs and symptoms almost always resolve spontaneously; usually, little or no treatment is required. Some delayed reactions may be coincidental. Pediatric patients (<18 yr) who were exposed to iodinated contrast media (ICM) were found to be at higher risk for iodine-induced thyroid dysfunction. The risk of incident hypothyroidism was found to be significantly higher following ICM exposure (OR 2.60, 95% CI 1.43 - 4.72, $p<0.01$). The median interval between exposure and onset of hypothyroidism was 10.8 months, and in hypothyroid cases, the median serum thyroid-stimulating hormone concentration was 6.5 mIU/L (interquartile range, 5.8-9.6). The authors noted that children receiving ICM should

be monitored for iodine-induced thyroid dysfunction, particularly during the first year following exposure [28].

A basic understanding of iodinated contrast media (ICM), the risks of their administration, the choice of the available agents, and premedication regimens for high-risk patients is beneficial in preparing patients for their contrast-enhanced imaging examinations. Radiologists are the primary physicians who administer contrast material. Because reactions to ICM may occur unexpectedly, radiologists should be able to recognize and treat the various types of possible adverse reactions, and they should seek clinical assistance as needed.

Thrombolysis in clinical practice

Pathophysiology of blood clots

Coagulation or blood clotting is a very important biological process which transfers the liquorish blood to solidify. It is fundamental to form blood clots when we have an injury that reaches the blood vessels. Clotting can prevent us from bleeding to death and protect us from the entry of bacteria and viruses. However, clots can also form inside our body, without surface injury, when a blood vessel is injured. The human body can make clots and breaks them down once there is no need for them anymore.

Mostly there is a healthy balance between these two activities. In some cases, abnormal blood clotting occurs; some people's body may not be able to break the clots down. On other hand, oversized clot inside a blood vessel is extremely dangerous because it can easily block the blood flow in the vessel. Thus, because of the lack of flow, indispensable organs will not obtain enough oxygen. These situations can be dangerous and require an immediate diagnosis and treatment. The blocked blood vessels can cause the followings:

- **Acute ischemic stroke** when the area of the brain doesn't have enough oxygen and nutrients
- **Deep vein thrombosis (DVT)** when the blood clot is formed in a vein deep in the human body. The most common case of DVT occurs in a lower leg or thing. It also can occur in other parts at the body
- **Pulmonary embolism (PE)** evolves when a blood clot in a deep vein breaks off and the fragments travel through the body. These pieces can go to an artery of the lung and block the blood flow
- **Heart attack** happens when the flow of the oxygen rich blood becomes suddenly blocked, so the heart is not able to get enough oxygen. The section of the muscle, if the flow cannot restart quickly, will start to die.

Mechanisms of Thrombolysis

Fibrinolysis refers to the dissolution of the fibrin network which was formed by the coagulation cascade to prevent bleeding [29]. This process has two isolated types: primary fibrinolysis and secondary fibrinolysis; the primary type is a normal body process. The secondary fibrinolysis or so called thrombolysis is a pharmacological dissolution of the fibrin thrombus by exogenously injected agents.

The main enzyme for breaking down blood clots is plasmin which is a proteo-lytic enzyme. It is capable of breaking cross-links between fibrin molecules, which provide the structural integrity of blood clots, leading to the production of circulating fragments which are cleared out from the vessels by the kidney and liver. Plasmin is produced in an inactive form, called plasminogen, in the liver. Although plasminogen does not have direct effect on fibrin, it still has an affinity for it, and conjugates into the clot when it is formed. Thrombolytic drugs dissolve blood clots by

activating plasminogen as well. Because of these actions, thrombolytic drugs are also called "plasminogen activators" and "fibrinolytic drugs" [30,31].

Thrombolytic drugs

There are three major classes of fibrinolytic drugs: tissue plasminogen activator (t-PA), streptokinase (SK), and urokinase (UK). While drugs in these three classes could effectively dissolve blood clots, they differ in their detailed mechanisms for dissolving blood clots. Tissue plasminogen activator (t-PA) and urokinase are the agents that convert plasminogen to the active plasmin, thus allowing fibrinolysis to occur.

Tissue plasminogen activator

Tissue plasminogen activator (t-PA) is a single-chain, 70 kDA, serine protease. The enzyme has four main parts: finger or F domain, growth factor or E domain, two kringle regions (K1 and K2), and a serine protease domain, which is –COOH terminated. This part has the active side on for the cleavage of plasminogen [1]. The two-finger domain are like the cringle domain on plasminogen, thus, their residues are responsible for fibrin affinity; they have fibrin-selective properties (**Figure 2**).

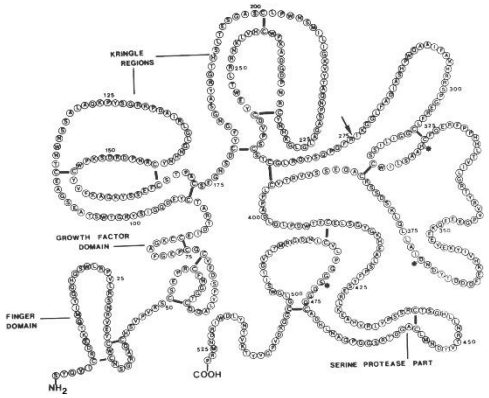

Figure 2: Representations of the amino acid sequence of t-PA [1]

The main of t-PA role is enhancing the conversion from inactive plasminogen to active plasmin. The activity of t-PA is greatly increased in the presence of fibrin, which also increase fibrinolysis specifically at the site of thrombosis. Because of the relative fibrin specificity of t-PA, clot dissolution occurs with less breakdown of circulating fibrinogen than occurs with SK and UK. Although t-PA is relatively selective for clot-bound plasminogen, it still activates circulating plasminogen thereby releasing plasmin, which can lead to the breakdown of circulating fibrinogen and cause an unwanted systemic fibrinolytic state. Normally, circulating α_2-antiplasmin inactivates plasmin, but therapeutic doses of t-PA (and SK) lead to sufficient plasmin formation to overwhelm the limited circulating concentrations α_2-antiplasmin. In summary, although t-PA is relatively selective for clot-associated fibrin, it can produce systemic lytic state and undesirable bleeding. Moreover, t-PA is released into the blood slowly by the damaged endothelium of the blood vessels. This occurs because plasminogen became entrapped within the clot during formation; as it is slowly activated, it breaks down the fibrin mesh step by step. Because of the prolonged release of the enzyme, it is possible that after several days the clot is not completely broken down. Besides, streptokinase is not a protease and has no enzymatic activity; however, it forms a complex with plasminogen that releases plasmin. Unlike t-PA, it does not bind preferentially to clot-associated fibrin and therefore binds equally to circulating and non-circulating plasminogen. Therefore, SK produces significant fibrinogen lysis along with clot fibrinolysis. For this reason, t-PA is generally preferred as a thrombolytic agent over SK, especially when used for dissolving coronary and cerebral vascular thrombi. Because SK is derived from streptococci, patients who have had recent streptococci infections can require significantly higher doses of SK to produce thrombolysis.

On other hand t-PA is inhibited by plasminogen activator inhibitor type 1 (PAI-1) in plasma. The capacity of PAI-1 to bind t-PA is quickly surpassed when the drug is administered systemically,

thus the risk of bleeding is much higher. The half-life of t-PA in the circulation system is about 4 minutes, it is cleared by the liver, but the physiological effect may last longer as a consequence of fibrin binding [1].

Specific Thrombolytic Drugs

Tissue Plasminogen Activators: this family of thrombolytic drugs is used in acute myocardial infarction, cerebrovascular thrombotic stroke and pulmonary embolism. For acute myocardial infarctions, tissue plasminogen activators are generally preferred over streptokitablenase.

- Alteplase (Activase®; rt-PA) is a recombinant form of human t-PA. It has a short half-life (~5 min) and therefore is usually administered as an intravenous bolus followed by an infusion.
- Retaplase (Retavase®) is a genetically engineered, smaller derivative of recombinant t-PA that has increased potency and is faster acting than rt-PA. It is usually administered as IV bolus injections. It is used for acute myocardial infarction and pulmonary embolism.
- Tenecteplase (TNK-t-PA) has a longer half-life and greater binding affinity for fibrin than rt-PA. Because of its longer half-life, it can be administered by IV bolus. It is only approved for use in acute myocardial infarction.

Thrombolytic therapy

Thrombolytic therapy is the treatment to break up or dissolve the clots in the circulation system, re-open the blocked vessels and improve the flow. The systematic administration of thrombolytic drugs is approved as an immediate treatment for stroke, DVT, PE or heart attack. The most commonly used drug is tissue plasminogen activator (t-PA). There are some key facts which make t-PA the optimal chose. For example, it's an FDA (Food and Drug Administration) approved drug;

it is possible to give in a vein and in some cases, may be given directly into an artery. The treatment might be beneficial for 6 hours. The patients' saving is greater with 26%, moreover, the disability free treatments are increased with 6% [32,33].

Even if the tissue plasminogen activator is a life-saving drug in many cases, not everybody can get t-PA. There are some restrictions such as: candidates who are older than 80 years; recent heart attack; head trauma within the last three months; bleeding disorders, pregnancy, [4].

However, the tissue plasminogen activator has some serious side effects. Intravenous t-PA given within 3 – to 6-hour time window show efficacy, but the benefit is, sometimes, smaller than risk of side-effect. The most serious side effect is bleeding. The bleeding occurred at the in the most critical locations such as intracranial, gastrointestinal, retroperitoneal, and pericardial. In this case, the therapy should be stopped immediately, and start along a therapy with heparin. Death and permanent disability are regularly reported in patients who have serious bleeding episodes, experienced stroke or intracranial bleeding.

A study of Activase, in acute ischemic stroke, suggested that doses higher than 0.9 mg/kg may relate to an increased number of symptomatic intracerebral hemorrhages (ICH). Doses is greater than 0.9 mg/kg, but not more than 90 mg, might not be applied for the management of acute ischemic stroke [34].

Other side effects of thrombolytic agents are possible like: blood in the urine, blood in the stool, or black, tarry stools, constipation, coughing up blood, nosebleeds, unexpected or unusually heavy vaginal bleeding, dizziness, sudden, severe, or constant headaches, pain or swelling in the abdomen or stomach, back pain or backache, severe or constant muscle pain or stiffness, stiff, swollen, or painful joints [35].

Role of Computed Tomography and Magnetic Resonance Imaging for Thrombosis

Computed Tomography vs. Magnetic Resonance Imaging for Thrombosis

During the 1990s, computed tomography (CT) and magnetic resonance (MR) imaging changed significantly due to the technological advancement and expanded clinical use in patients with thromboembolic disease, particularly with regard of the pulmonary vasculature, acute ischemic stroke, deep vein thrombosis, pulmonary embolism or heart attack. In countless institutions, helical CT pulmonary angiography has become the basic imaging study choice to evaluate patients with suspected thrombolysis. In addition, CT venography of the pelvis and lower extremities is often incorporated into the CT angiography protocol to identify or exclude concurrent deep venous thrombosis.

Although MR imaging produces high tissue contrast without ionizing radiation, currently, this technique is less popular than CT for evaluation of acute venous thromboembolism (VTE) because of technical limitations, higher costs, limited availability, and other logistical considerations. As technology improves, however, MR pulmonary angiography (MRPA) and MR venography (MRV) may play a greater role in the evaluation of patients with venous thromboembolic disease.

Negative side effect of iodinated contrast media for thrombolysis

Iodinated contrast media are widely used either to visualize blood vessels (angiography) or to increase the density between different organs and tissues. In both cases, they are infused intravascularly and theoretically, there is no interaction between media and other presenting drugs [36]. However there is a concern for a possible interaction between x-ray contrast agents and thrombolytic therapy [37-39]; since contrast enhanced computed tomography (CT) evaluation is performed prior to rt-PA administration for localizing a thrombus [40] and this multi-phase approach

provides greater information than non-contrast CT alone. Clinical data from the cardiology literature propose that rt-PA induced thrombolysis in the presence of both ionic and nonionic iodinated contrast agents notably slows down [41]. However, in current clinical practice, the interaction between contrast agents and fibrinolysis is marginal due to the importance of the mechanical recanalization techniques.

Iodinated contrast agents may be non-ionic or ionic, and they all have different physical parameters such as viscosity at 20 ºC and 37ºC or osmolality of the soliton in which they are provided. Numerous methods were established to develop an in-vitro clot lytic model for understating the effect of ionic and nonionic iodinated contrast agents on rt-PA; notwithstanding the most reliable way to investigate clot lysis activity of rt-PA is through vitro clot lysis model [42-44]. Previously, Basta et al [45] used ultrasound methods to measure the thrombolytic activity of streptokinase on artificial clots. Several other cases have been published which describes either clinical statistical data [46] or introducing case studies [47]. However, these approaches might contain the differences of patients such as age, gender, medical history or lifestyle.

Nanotechnology

What is nanotechnology?

Most definitions revolve around materials at length scales below 100 nm and quite often they make a comparison with a human hair, which is about 80,000 nm wide. Also, the U.S. National Nanotechnology Initiative (NNI) provides the following definition [33]:

"Nanotechnology is the understanding and control of matter at dimensions between approximately 1 and 100 nanometers, where unique phenomena enable novel applications. Encompassing nanoscale science, engineering, and technology, nanotechnology involves imaging, measuring, modeling, and manipulating matter at this length scale."

Brief history of nanotechnology

The history of the nanotechnology started in 1959 when Richard Feynman introduced the idea of nanotechnology in his famous talk "*There's plenty of room at the bottom*" at the annual meeting of the American Physic Society. Feynman proposed employing machine tools to make smaller machine tools, and those machine tools would be used to make more smaller machine tools; all the way down to the atomic level [48]. Feynman was clearly aware of the potential medical applications of this new technology. He proposed the first nano-robotic surgical procedure to cure heart disease: "… *a friend of mine (Albert R. Hibbs) suggests a very interesting possibility for relatively small machines. He says that, although it is a very wild idea, it would be interesting in surgery if you could swallow the surgeon. You put the mechanical surgeon inside the blood vessel and it goes into the heart and looks around. It finds out which valve is the faulty one and takes a little knife and slices it out. That we can manufacture an object that maneuvers at that level! Other small machines might be permanently incorporated in the body to assist some inadequately functioning organ*" [32].

He imaged a new technology which might allow the scientists to manipulate the materials at its basic elements: the single atoms. A few years later, in 1974, Norio Taniguchi named this filed to nanotechnology. Despite of the fact that scientists applied this design for years, nanotechnology became an individual scientific field just in 1981. Since then, 35 years of research and development, nanotechnology infiltrates in almost every field of science and industry, from biology to construction science, including electronic and environment control [49-52]; bringing new promises into each field. Nanotechnology is a revolutionary way of understanding technology and manufacturing in different sectors of industries such as transportation, nuclear weapons, detection systems, and telecommunications.

However, we need to understand deeper the mechanism of nanostructures, because the complexity of the systems is not fully cleared. The invention of the Scanning Tunneling Microscope (Gerd Binnig and Heinrich Rohrer, won the Nobel Prize in Physics, 1986) allowed the visualization of single atoms; in 1985 Smalley and his group synthetized the first artificial molecular compound (C_{60}, the fullerene, which worth them the Nobel Prize in Chemistry in 1996) [53].

Principles of nanotechnology

Nanomaterials

Nanomaterials are the different materials that have been designed to have one, two or three dimensions in nanoscale. These include components like carbon wires and tubes, and even small mechanical devices. This nanoscale world is magnificently small – one nanometer is a millionth of a millimeter. To put this into practice, a string of DNA is 2.5 nm wide; a red blood cell is 7,000 nm across or a human hair is 80,000 nm wide, a dust mite is 200 um – surprisingly, even if these everyday things are miniature, they are still but larger than nanomaterials (**Figure 3**) [54].

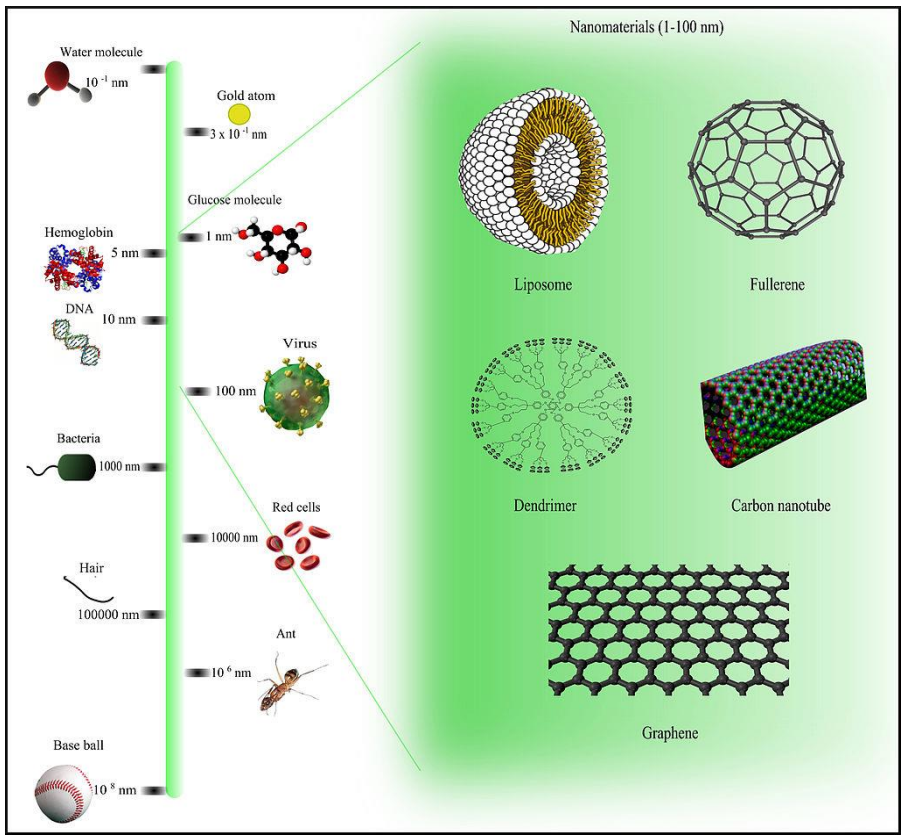

Figure 3: Demonstrating nanosize [46]

While many of these unexplored properties might be useful, using nanomaterials can also product new risks. Nanomaterials have a great surface area compared to their bulk analogues (**Figure 4**). This typically follows in greater chemical reactivity, biological activity and catalytic behavior compared to larger particles of the same chemical composition [55-57]. Nanomaterials may also more willingly penetrate into biological membranes and penetrate cells, tissues and organs of living organisms [56,58]. This can be highly desirable for therapeutic purposes but unfavorable when unintentional exposure occurs.

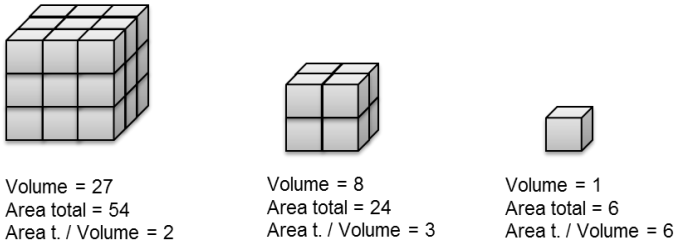

Figure 4: Surface area of different size of nanoparticles

Nanomedicine

The application of nanotechnologies to medicine is one of the most promising fields where nanotechnologies may strongly improve medical practice for prevention and therapeutic purposes. Nanomedicine includes several distinct application areas: in vitro diagnostics, drug delivery, in vivo imaging, radiopharmaceuticals, and active implants. There are altogether 86 subcategories, and each subcategory may have countless of projects, applications [32]. I will briefly describe only a few of the most interesting research ideas:

- Immuno-isolation: Deasi et al [59] created one of the first and simplest medical device, however the idea was fascinating. They performed a surface with holes or nanopores on a chamber. These holes were 20 nm in diameter; the pores were large enough to assign small molecules such as oxygen, glucose, insulin, or ions. The chamber interfaced with the surrounding biological environment. However, the holes prevented the passage of the large immune cells. Behind the barrier, they placed encapsulated rat pancreatic cells, connected with the nutrients, and these cells live for weeks, thus they could secrete insulin, but they remained hidden form the immune system. In this way, the immune system was not able to attack and destroy the foreign cells, like it normally would have been occurred [60].

- Fullerene-based pharmaceuticals: Soluble derivatives of fullerene, such the most famous C_{60}, the soccer-ball shaped composition of 60 carbon atoms, have a great engagement with

pharmaceutical agents. They can encapsulate drug in the center of the ball; highly biocompatible, and have a low toxicity, even if the amount of the drug is large [61]. Nowadays the leading company is C-Sixty (www.csixty.com).

- Microfluidics: in the micro world, flows which are driven by differences of pressure become extremely inefficient (due to the forth of the radius of the pipe), compared to capillary absorption or concentration gradient flow. Microfluidics plays a fundamental role in different fields and applications, such as the fabrication of microprocessor or blood cells flowing in a capillary.

- Nanorobots: The nanorobot expression means the engineered or artificially constructed microorganisms, which genome are reduced to the minimum size. In the medicine, these synthetic microbes metabolize non-toxic end products such as vitamins, hormones, enzymes or proteins which the patient's body was deficient. Moreover, these robots could selectively absorb toxic substances like toxins, or indigestible intracellular products. This field is new; thus, we look forward to witnessing the first clinical trial.

Metallic based nanoparticles

Presently, the group of the most important nanomaterials includes simple metal oxides such as titanium oxide (TiO_2), zinc oxide (ZnO), magnesium oxide (MgO), copper oxide (CuO), aluminum oxide (Al_2O_3), manganese oxide (MnO_2) and iron oxide (Fe_3O_4, Fe_2O_3) [62-66]. Metal oxide based NPs are finding increasing application in a wide range of fields and represent about one-third of the consumer products of nanotechnology market [67]. For example these materials are used as pigments in paints (TiO_2), or sunscreens and cosmetics (TiO_2, ZnO), or antimicrobial agents (MgO, CuO), in industrial operations (Al_2O_3, MnO_2) and for medical purposes (Al_2O_3, Fe_3O_4, Fe_2O_3) [62-66]. Aluminum nanomaterials act as drug delivery systems, by encapsulating the drugs the

drugs to increase solubility for evading clearance mechanisms and allowing the site-specific targeting of drugs to cells [68]. Previous toxicological studies on nanomaterials were conducted on TiO_2, CdO_2, C_60, and carbon nanotubes only [62]. Although the toxicity of iron oxide nanoparticles (IONPs) is well established, they are the only metal oxide nanoparticles approved for clinical use, has been investigated only in a small number of studies.

Introduction to Magnetic Nanoparticles

Several fields utilize the properties of magnetic nanoparticles (MNPs) in various biochemical and biomedical applications including bacterial detection, protein purification, enzyme immobilization, cell separation, drug delivery, hyperthermia, and MRI imaging. Magnetic nanostructures are well-established nanomaterial with controlled size, ability to be manipulated by an external magnetic field, and enhancement of contrast in magnetic resonance imaging. The core component for synthetizing MNPs is colloidal magnetite or hematite (Fe_3O_4) [69 70].

Iron and its compounds are widespread in nature and successfully synthesized in the laboratory. Iron compounds present in the hydrosphere, the lithosphere and (as pollutants) in the atmosphere. Iron is a biogenic element, present in all biota, but some iron compounds can cause harmful effects to humans, animals, and environment [71,72]. In occupational exposure of humans, iron and iron oxides are known to produce benign siderosis – but iron oxides have been implicated also as a vehicle for transporting high concentrations of carcinogens and sulfur dioxide deep into the lungs, thereby enhancing the activity of these pollutants [71]. There are existing 6 iron oxides which composed Fe_2O_3: hematite (α-Fe_2O_3), magnetite (Fe_3O_4), maghemite (γ-Fe_2O_3), β-Fe2O3, ε-Fe_2O_3 and Wüstite (FeO). In most of these compounds, iron is in the trivalent state, but FeO and Fe_3O_4 contain Fe(II) [72].

- Hematite, α-Fe_2O_3, is the oldest known Fe oxide mineral and is widespread in rocks and soils. It is extremely stable and is often the final stage of transformations of other iron oxides. The blood-red-colored hematite is an important pigment and a valuable ore. Other names for hematite include iron(III)oxide, ferric oxide, red ochre and kidney ore.
- Magnetite, Fe_3O_4, is a black, ferromagnetic mineral containing both Fe(II) and Fe(III). Magnetite is an important iron score. Together with titan magnetite, it is responsible for the magnetic properties of rocks. It is formed in various organisms in which it serves as an orientation aid. Other names for magnetite include black iron oxide, magnetic iron ore, iron (II, III) oxide and ferrous ferrite.
- Maghemite, γ-Fe_2O_3, is a red-brown, ferromagnetic mineral isostructural with magnetite, but with cation deficient site. It occurs in soils as a weathering product of magnetite or as the product of heating of other Fe oxides, usually in the presence of organic matter [72]

The synthetic control of the monodispersed of the iron oxide nanoparticles is crucial because their properties depend greatly upon the size and shape of the nanoparticles. To understand and thus fully utilize the potential of ferrofluids, careful studies examined its physical behavior in terms of stability, surfactants, particle sizes, and materials are essential [72-74] . The colloidal characteristics which allow for the biological application of iron oxide nanoparticles are determined by their surfaces and not by their bulk volume [75]. A traditional textbook definition of a colloid is a suspension of finely divided particles of one material in a dispensing medium that do not separate on long-standing [76,77]. The phenomena of colloidal stability originate from thermal motion or Brownian motion where random collisions with other particles, suspending fluid, or container wall cause continuous redirecting of a particle's trajectory that resist sedimentation. However, magnetic nanoparticles due to van-der Walls and magnetic dipole–dipole attractive forces have tendency to

coagulate which results in a decline in their colloidal stability, aggregates of increasing size, and eventual gravitational sediment. To achieve colloidal stability in a biological environment (pH, osmolality) a balance must be maintained between the inter-particle van der Waals attractive forces and the 3 electrostatic repulsion based on surface charge [78]. This goal can be accomplished by the formation of an electric double layer on the nanoparticle following synthesis [79]. The ability to manipulate the unique magnetic properties of iron oxide nanoparticles also make them highly desirable for biomedical applications. These properties are largely determined by the chemical composition, size, and shape of the particles. Nevertheless, the extent to which these factors can be completely controlled is variable. Thus the properties of the same type of magnetic nanoparticle may not be consistently reproducible [73].

The two most commonly studied iron oxides have been magnetite (Fe_3O_4) and maghemite (γ-Fe_2O_3) [72]. IONPs are found naturally in the environment as particulate matter in air pollution and in volcanic eruptions. Either Fe_3O_4 (magnetite) or γFe_2O_3 (maghemite), particles can be generated as emissions from traffic, industry and power stations but can also be specifically synthesized chemically for a wide variety of applications [80-82]. Various methods can be employed in their fabrication such as synthesis by water-in-oil micro-emulsion system, co-precipitation, reactions in constrained environments, polyol method, flow-injection synthesis and sonolysis [80-82]. Magnetic behavior is an important parameter in design and synthesizing of superparamagnetic iron oxide NPs (SPIONs) to maximally facilitate their imaging and therapeutic efficacy as these applications require high magnetization values. Although this can be accomplished by applying a maximum magnetic field acceptable under the clinical settings, the reaction conditions during the synthesis processes can be modulated to generate particle size with a large surface area, which in turn allows these particles to exhibit high magnetic susceptibility [76,77,83]

Iron in the human body

The content of iron in the human body is regulated by a complex mechanism for maintaining homeostasis. During childhood, pregnancy or blood loss, the need for iron is increased and so is the absorption. Absorption occurs in two steps: absorption of ferrous ions from the intestinal lumen into the mucosal cells, and transfer from the mucosal cell to the plasma, where it is bound to transferrin for transfer to storage sites. Transferrin is a β1-globulin and is produced in the liver. As the Fe2+ ion is released into plasma, it becomes oxidized by oxygen in the presence of ferroxidase I. There are 3–5 g of iron in the body, about two-thirds of which is bound to hemoglobin, 10% to myoglobin and iron-containing enzymes, and the remainder is bound to the iron storage proteins ferritin and hemosiderin. Exposure to iron induces synthesis of apoferritin, which then binds ferrous ions. The ferrous ion becomes oxidized, 7 probably by histidine and cysteine residues, and by carbonyl groups. Iron may be released slowly from ferritin by reducing agents such as ascorbic acid, cysteine, and reduced glutathione. Normally, excess ingested iron is excreted, but some remains within shed intestinal cells, in bile, in urine, and in even smaller amounts in sweat, nails, and hair. Total iron excretion is usually ~ 0.5 mg/day. With excess exposure to iron or iron overload, there may be a further increase in ferritin synthesis in hepatic parenchymal cells. In fact, the ability of the liver to synthesize ferritin exceeds the rate at which lysosomes can process iron for excretion. Lysosomes convert the protein from ferritin to hemosiderin, which then remains in situ. The formation of hemosiderin from ferritin is not well understood, but it seems to involve denaturation of the apoferritin molecule. With increasing iron loading, ferritin concentration appears to reach a maximum and a greater portion of iron is found in hemosiderin. Both ferritin and hemosiderin are, in fact, storage sites for intracellular metal and are protective in that they maintain intracellular iron in bound form. A portion of the iron taken up by cells of the

reticuloendothelial system enters a labile iron pool available for erythropoiesis, and part becomes stored as ferritin [71].

Magnetic Domains

The magnetic property of specific interest, to this study, termed superparamagnetic, occurs in particles below 30nm in size. As constrained by their size, in theory these nanoparticles contain a single magnetic moment or domain; a summation of all the individual magnetic moments (motion) of the electrons of all the iron atoms the particle contains. A magnetic material is made up of small regions known as magnetic domains that form as the material develops its crystalline structure during synthesis. In each domain, all the atomic dipoles are coupled together in a preferential direction. This magnetic moment will naturally orient itself in the most stable direction due to its magnetic anisotropy that is determined by the atomic crystalline structure and shape (edge regularity) of the nanoparticle. It is important to recognize that magnetic domains are not analogous to the physical, crystallographic domains, as magnetic domains cannot be viewed with non-magnetic imaging techniques [84].

Clustered Iron Oxide Nanocubes

Iron oxide nanocrystals (IOs) have a great promise as agents for magnetic resonance imaging (MRI), localized hyperthermia treatment, controlled drug release, magnetic guidance and manipulation. Typically, the core size of the iron oxide particles is around 30 nm; and they are encapsulated to the core of the nanoparticles. This configuration can be used for localized hyperthermia, tissue thermal ablation, and controlled drug release from nanoparticles; achieved by exposing IOs to alternating magnetic fields (AMFs) for sufficiently long periods of time. Moreover, static magnetic fields can suitable for remotely guide IOs to specific biological targets and non-invasively manipulate molecules and cells. On other hand, several papers proved that IOs are biodegradable and the dissolved iron can physiological metabolized by cells. Hence, limiting possible toxicity concerns and supporting repetitive use. The intrinsic theragnostic properties, biocompatibility, and biodegradability have contributed to the popularity and success of IOs in biomedical applications.

Magnetic hyperthermia of iron oxide nanocubes (NCs)

Magnetic hyperthermia is the name given to an experimental treatment. It is because magnetic nanoparticles, when exposed to an alternating magnetic field (AMF), can generate heat. The energy from the field drives the magnetic moments to rotate and aligns them with the magnetic field direction by overcoming the thermal energy barrier. Once the external magnetic field is removed, magnetic moments do not relax immediately but rather take some time to randomize their orientations. This heat dissipation can be due to rotation of the entire magnetic particle within a surrounding liquid medium (Brownian relaxation) and/or to rotation of the magnetic moment within the magnetic core (Neel relaxation) [85] . Again, the particle composition, shape, size, as well as the concentration and viscosity of the suspension medium, and the magnitude and frequency of the applied magnetic field determine the relative influence of each of these inductive heating

mechanisms. It is generally inferred that the internal Neel mechanism dominates particles with diameters below 20 nm while larger particles generate heat through the external Brownian rotation mechanism [86] Therefore, if targeted magnetic nanoparticles are injected to a patient and this patient is placed in an alternating magnetic field of well-chosen amplitude and frequency, the temperature around the nanoparticles, which are accumulated to at the targeted area, would rise. This increasing temperature can help i) to penetrate the drug into the organ ii) activate the nanoparticles iii) kill the bacteria (if there is any infection in that area) iv) destroy tumor cells.

Countless magnetic materials have a magnetic hysteresis when subjected to a magnetic field. The volume of this hysteresis loop is disposed to the environment as thermal energy, and this is the energy utilized for magnetic hyperthermia. The power disposed by the magnetic material exposed to an alternating magnetic field is called the "Specific Absorption Rate" (SAR); it is expressed in W/g of nanoparticles. The SAR of the magnetic material is given by SAR = Af, where A is the area of the hysteresis loop and f the alternation frequency of the magnetic field. A is expressed in J/g and is called the "specific losses" of the material. Note that this expression for SAR is just a definition; the difficulty lies in finding A. A depends on all the properties of the magnetic material in a very complex aspect. In the case of magnetic nanoparticles, A depends on their magneto crystalline anisotropy K, their volume V, the temperature T, the frequency of the magnetic field f, its amplitude H_{max}, and on the volumic concentration of the nanoparticles [87,88].

Specific absorption rate (SAR) measurement for hyperthermia

Magnetic heating property of iron oxide NCs is measured by hyperthermia system. The measurement is examined by using a radio frequency generator producing an alternating magnetic field (AMF) with a frequency (*f*) of 512 KHz and field amplitude (H) of 10KA/m. Cooling system thermally isolated the vial from the high temperature of the coil when applying AMF. Magnetic

iron oxide NCs suspension is placed in a cylindrical probe (4 mm ID x 40 mm height). Temperature is monitored with an optical probe (OptiSens Instrument) immersed into the geometrical center of the solution. When the sample suspension reaches to the equilibrium temperature (~19 °C), the field is switched on and temperature changes are recorded every sec for about 15-20 minutes. The specific absorption rate (SAR) was calculated based on the formula of (1):

$$SAR = \frac{\Delta T}{\Delta t}\Big|_{t=0} C_p \frac{1}{m_{Fe}} \qquad (1)$$

where T is the temperature of the nanocube suspension; t is the time; Cp is the heat capacity of the buffer; m_{Fe} is the final mass fraction of the iron in the sample suspension.

Biomedical Application of the Magnetic Properties of Nanoparticles

Biomedical applications of iron oxide nanoparticles SPION have some unique physio-chemical features, such as nanometer sizes and a large surface area to mass ratio that also facilitate novel applications [89]. Nanomaterials inhabit the realm where the size of the largest biological molecules and the smallest manmade probes meet, allowing for nanomaterials to be utilized with in vitro (protein and cell detection and separation) and in vivo (drug and therapy delivery and imaging) aims in interdisciplinary biomedical fields [70,90]. Due to their magnetic properties SPIONs have been extensively used in a number of bio applications including magnetic drug and gene delivery [91], tissue repair, cell separation [72], magnetic resonance imaging [92,93] and magnetic fluid hyperthermia [84] [83,94,95]. An exciting field within the magnetic nanoparticle field, termed 'nanobiomagnetism' takes advantage of their unique, size-dependent properties at the juncture of nanomagnetic and medicine where the magnetic-field responsive nanoparticles can be used as medical and surgical instruments [96]. The applications that relate specifically to the work discussed

in this dissertation involve the utilization of the both the diagnostic and therapeutic potential of superparamagnetic iron oxide nanoparticles.

Diagnostic In Vivo Imaging

In the field of bio-imaging, the use of magnetic nanoparticles as contrast agents has proved useful as their longer renal clearance time and higher relaxation values are of advantage when compared to traditional gadolinium-based contrast agents [97]. This contrast enhancement using superparamagnetic iron oxide nanoparticles (SPIONs) is a consequence of their superparamagnetic, the magnetic moments within the SPIONs align in the direction of the field, this gives rise to a large net magnetic moment, in comparison, paramagnetic material exhibit only a small net magnetic moment [98]. The large magnetic moment generated by SPIONs leads to a disturbance in the local magnetic field, causing a shortening of the hydrogen nuclei relaxation times. The water protons adjacent to the particles react to this inconsistency in the field by increasing their relaxation rate, thus generating a strong reduction of T2 relaxation time (dark, negative T2 contrast) and a relative small influence on T1 relaxation time are the consequences [99,100]. This shortening in proton relaxation times leads to a detectible change in the T2 MRI signal. Currently there are two FDA approved SPION contrast enhancement agents, Endorem® EU (Ferridex USA) and Resovist® (Schering AG), both used for liver and spleen imaging. Sinerem EU (Combidex USA) is another SPION contrast agent currently in phase III trial for application in lymph node imaging [101].

Therapeutics

SPIONs are bridging the therapeutic gap that remains due to the limitations of conventional drug delivery systems. In attempts to overcome issues inherent to conventional chemotherapy (inadequate chemotherapy dosages reaching the tumor site, severe cytotoxicity, and tumor

resistance, nanoparticles are loaded or doped with biological or pharmaceutical agents. Then iron oxide particles carriers can be guided to the desired target area using an external magnetic field or by specifically-tagging the nanoparticles with tissue-specific 6 antibodies. Once the SPIONs are concentrated at the target site, they can be released through remotely-induced enzymatic activity, changes in physiological conditions, or temperature [102,103]. While these applications regard nanoparticles as secondary transporters of chemotherapeutic agents, one area of therapy focuses on the intrinsic superparamagnetic properties of the iron oxide particles a primary source of cytotoxicity.

Introduction to Tumor Hyperthermia

With the possibility to convert dissipated magnetic energy into thermal energy, the application of magnetic materials for hyperthermia treatment of cancer was first proposed in 1957 [104]. Since then the approach evolved into a well-researched field due to the introduction of magnetic nanoparticles (MNPs). MNPs-based hyperthermia treatment has several advantages compared to conventional hyperthermia treatment. These are:

i. cancer cells absorb MNPs thereby increasing the effectiveness of hyperthermia by delivering therapeutic heat directly to them
ii. MNPs can be targeted by means of cancer-specific binding agents making the treatment much more selective and effective
iii. MNPs can also effectively cross blood-brain barrier and hence can be used for treating brain tumors [105],
iv. effective and externally stimulated heating can be delivered at cellular levels through alternating magnetic field [106],

v. the possibility to obtain stable colloids using MNPs, they can be administered through a number of drug delivery routes [80,81]

vi. MNPs-based hyperthermia treatment may induce antitumoral immunity [106]

vii. last but most important aspect is that MNP-based hyperthermia can also be utilized for controlled delivery of drugs and the first such nanoconstruct for this purpose has been made using layer-by-layer self-assembly approach [107]

Cancer cells are susceptible to heat which decreases their viability and increases their sensitivity to chemotherapy and radiation. Tumor vasculature, depending on tumor type, often is inadequately developed, thus the tumor cannot sufficiently be cooled by blood flow. The cancer therapy, hyperthermia, takes full advantage of this Achilles' heel of tumor cells, by raising the temperature of the target tissue to between 42 and 47°C [104,108]. While there are several methods that have been employed in the past to achieve this end, a discussion of the current and future state of intracellular cancer hyperthermia will best serve this dissertation.

Harnessing the Potential of Superparamagnetic and the Inductive Heating Phenomena

As mentioned earlier, magnetic fluid hyperthermia involves dispersing magnetic particles throughout the target tissue followed by the application of an alternating magnetic field of the necessary strength and frequency to cause the particles to heat by magnetic hysteresis losses or Néel relaxation. The investigation of the application of magnetic nanomaterials for hyperthermia gained attention with Gilchrist in 1957 who studied the bulk heating of tissue samples with iron oxide nanoparticles in the 20-100nm range [104]. More recently, cellular magnetic particle hyperthermia has become an attractive prospect because it offers a controlled modality by which there can be selective heating of target cell types by way of targeted nanoparticles. In addition the

cellular route of administering magnetic nanoparticles could selectively heat systemically-dispersed metastases as well as bulk tumor tissue [109].

Nanotheranostics

Generally, theranostics combines the imaging and treatment of disease into a single formulation. Most interesting are the theragnostic nanoparticles that combine imaging and treatment into a single nanomedical platform. The biocompatible and magnetic attributes of superparamagnetic iron oxide nanoparticles make them ideal candidates to overcome biological barriers, poor bio distribution of drugs, metastatic disease, drug resistant tissues, and ineffective treatment management [110]. The newest frontier in nanomedicine has been coined ‘nanotheranostics’ by which the diagnostic imaging and therapeutic capabilities of iron oxide nanoparticles are used in conjunction with their abilities to act secondarily as drug-carriers or as the primary chemotherapeutic agent; exploiting their intrinsic superparamagnetic properties [105]. The combined process of diagnosis and therapy into one process, a see-and-treat strategy, is at the forefront of a wave of personalized nanomedicine and the focus of this dissertation [111].

5. Results

Interactions between iodinated contrast media and tissue plasminogen activator: in vitro comparison study[112]

Materials and methods

Ethics Statement

The investigation conforms to the Guide for the Care and Use of Laboratory Animals published by the U.S. National Institutes of Health (NIH Publication No. 85-23, revised 1996), and was approved by the Animal Research Review Committee of the University of Pecs, Medical School.

Blood collection and clotting

Forming the rat blood clots, the blood was drawn from 8-10-month-old male WKY-strain Wistar Kyoto rats (Charles River Laboratories, Budapest, Hungary). Blood was obtained from the tail vein using a 25-gauge needle and 1mL syringe. 100 µl of blood was then aliquoted into several tubes which were containing 50U thrombin solution [113,114]. The tubes were placed for 3 hours at 37°C to form the blood clots than the clos were aged for 3 days at 4°C [115].

In vitro thrombolysis

The rt-PA was obtained from the manufacturer (Activase, Genentech, San Francisco, CA) as a lyophilized powder. The powder was mixed with sterile water to a concentration of 1 mg/mL as per the manufacturer's instructions. Thrombolysis was performed by placing individually the prepared clots in a 15 mL Falcon tubes. The tubes were containing 5.0 mL saline buffer, 100 µg rt-PA and different contrast media Xenetix® (iobitridol), Ultravist® (iopromide), Omnipaque® (iohexol), Visipaque® (iodixanol) and Iomeron® (iomeprol) (see **Table 1**). The quantity of each contrast media was chosen to study the effect of 30 mg or 60 mg iodine, the active substance, for the clot lysis. The dosages were calculated based on the manufactures' given ranges for an

average adult patient for intravascular administration. As a reference, there were vials containing 5.0 mL saline buffer and 100 µg rt-PA solutions (positive control) or just 5 mL saline solution (control). For each group, there were 5 clots.

Table 1.: The physical parameters of the iodine containing contrast media which were used in the current study. *The dosages given below are recommendations only and represent common doses for an average normal adult weighing 70 kg. Doses are given for single injections or per kilogram (kg) body weight (BW) as indicated below, based on the manufactures' instructions for Intravascular Administration

	Concentration of Iodine [mg I/mL]	Brand	Dosage*	Osmolality [mOsm / kg H_2O]	Viscosity [mPa s] 37°C	Active Substance
ULTRAVIST	300	Bayer AG	3 – 5 mL per kg body weight	607	4.7	iopromide
IOMERON	300	Bracco S.p.A.	3 – 5 mL per kg body weight	521	4.5	iomeprol
OMNIPAQUE	350	GE Healthcare	2.5 – 4 mL per kg body weight	844	10.6	iohexol
VISIPAQUE	320	GE Healthcare	3 – 4.5 mL per kg body weight	290	11.4	iodixanol
XENETIX	300	Guerbet Corporate	3 – 5 mL per kg body weight	915	10.0	iobitridol

The vials were placed into the incubator at 37°C and continuous shaking at 100 rpm for 90 minutes. The OD_{415} (optical absorbance) of the supernatant was measured (plate reader) at time point 0 min, 30 min, 60 min and 90 min to estimate the amount of released hemoglobin at 415 nm [116].

Statistical Analysis

Values are expressed as mean ± standard error and examined by one-way analysis of variance (ANOVA) and Tukey's HSD test. Statistical significance was declared at $P < 0.05$. All the analyses were performed by MINITAB Release 14.13.

Results

In Vitro thrombolytic efficacy of 30 mg active substance

Fig. 5 shows representative images of blood clots at 0 and 90 min, incubation with thrombolytic agent (positive control) or saline solution (negative control). These images clearly show the progressive lysis of the clots treated with rt-PA, since rt-PA breaks down the fibrin mesh releasing the red blood cells and inducing a progressive red coloration of the solution. For the assay, the thrombolytic efficacy was quantified by measuring the optical density (OD_{415}) of the supernatant at different time points, namely 0, 30, 60, and 90 minutes while the clots were treated different contrast media such as Xenetix® (iobitridol), Ultravist® (iopromide), Omnipaque® (iohexol), Visipaque® (iodixanol) and Iomeron® (iomeprol). Two different amounts of the contrast media

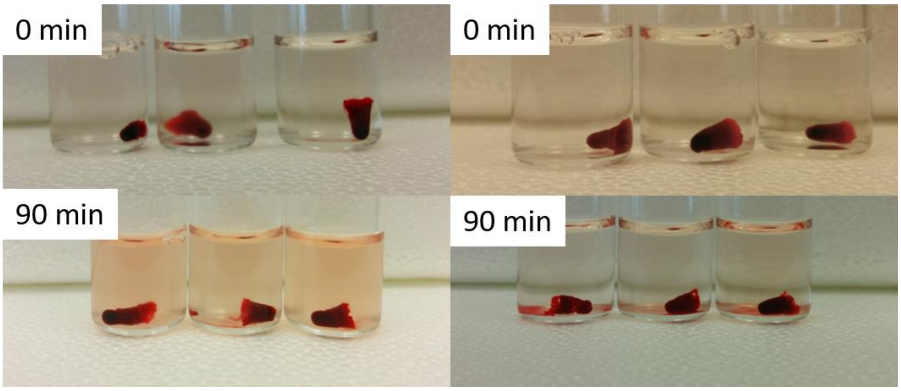

Fig. 5. Blood clot dissolution under static conditions. Representative images clot lysis of blood samples of Wistar Kyoto rats by 100 µg rt-PA (left) and saline solution (right).

were used for quantifying the rt-PA efficacy in dissolving blood clots over time: 30 mg or 60 mg

of iodine. Dissolution rate, which measures the dissolution velocity, are plotted in **Fig. 6** and **Fig. 7**, as a function of time for the different experimental groups.

As expected, only a minor dissolution of the untreated clot (negative control) is observed over time, related to a spontaneous break down of the fibrin network. To properly evaluate the results, a one way analysis of variance (ANOVA) and Tukey's HSD test [117] was conducted to compare the different time points for each experimental group. Firstly, we performed the statistical analysis for the 30-mg iodine group comparing the dissolution rates at each time points for each contrast media, positive and negative control separately.

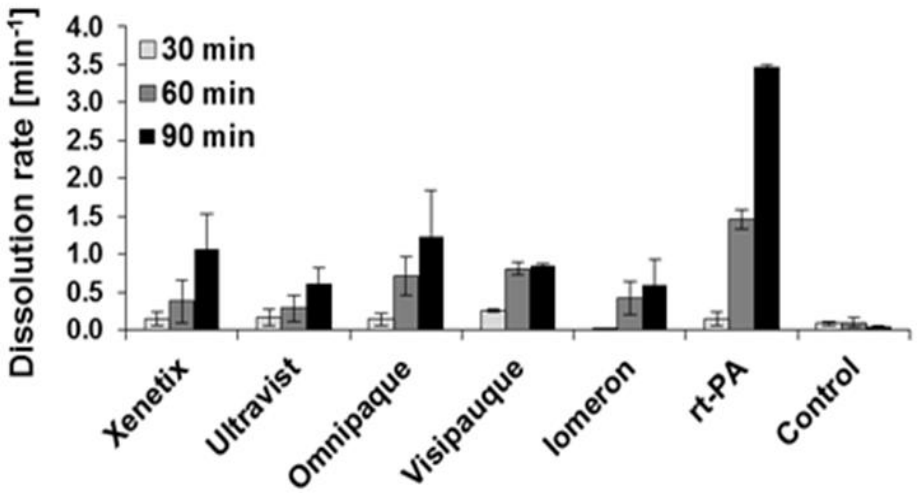

Fig. 6. Dissolution rate of blood clots over time exposed to 100 µg rt-PA in presence the five most commonly used contrast media (Xenetix® (iobitridol), Ultravist® (iopromide), Omnipaque® (iohexol), Visipaque® (iodixanol) and Iomeron® (iomeprol)); each in a concentration of 30 mg of active substance. After 30 minutes, there is a significant 56.2 ± 15.6%) drop in dissolution rate for the iodine containing groups comparing to the only rt-PA treated group.

We analyzed the performance of each contrast media containing group comparing to each other and the positive control group. For the first 30 minutes, there was no significant difference between the groups with contrast media and positive control. In the following time period, significant difference was found between all the contrast media groups and the positive control: a 56.2 ± 15.6% increase of dissolution rate was noticed for the positive control group compared to all the other samples (**Fig. 7**). With other words, rt-PA itself provides three orders of magnitude higher dissolution rate than clots treated with Xenetix® (iobitridol), Ultravist® (iopromide), Omnipaque® (iohexol), Visipaque® (iodixanol) and Iomeron® (iomeprol).

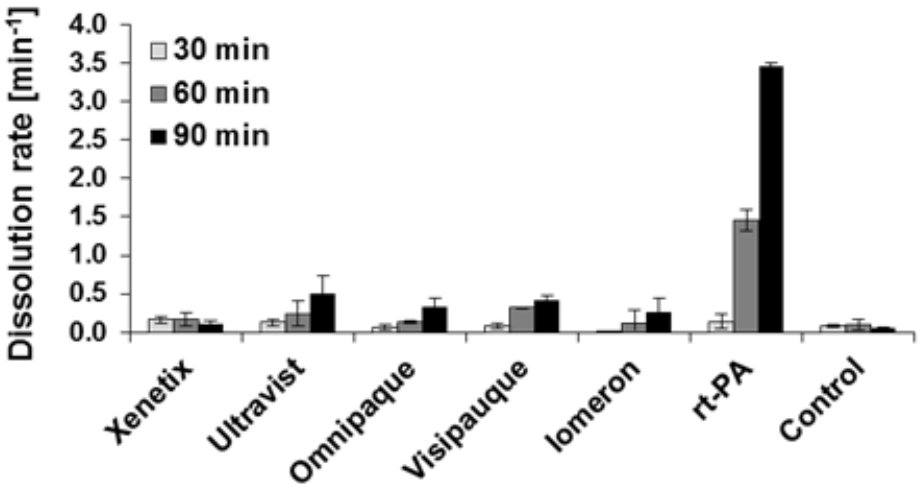

Fig. 7. Dissolution rate of blood clots over time exposed to 100 µg rt-PA in presence the five most commonly used contrast media (Xenetix® (iobitridol), Ultravist® (iopromide), Omnipaque® (iohexol), Visipaque® (iodixanol) and Iomeron® (iomeprol)); each in a concentration of 60 mg of active substance (iodine). After 30 minutes, there is a major (82.3± 23.9%.) drop in dissolution rate for iodine containing groups comparing to the only rt-PA treated group

In Vitro Thrombolytic efficacy of 60 mg active substance

The following step was to analyze the 60-mg group. The same analyses were performed. Fist we confirmed that in the rt-PA treaded groups the clot dissolution was successful, some hemoglobin was released. Next, we evaluated each contrast media containing group comparing to each other

and the positive control group, and we noticed that same trend as at 30 mg group. Namely, there were no significant differences between the contrast media containing groups, and all the rt-PA containing groups acted similarly in the first 30 minutes. In comparison, the positive control could provide ~100 times higher dissolution rate after the first 30 minutes compared to groups with contrast media (**Fig.7**).

DISCUSSION

This study shows in vitro dissolution of clots in presence of five different iodinated contrast media by rt-PA, assayed by an in vitro clot lysis model designed in our laboratory. Other research groups have studied the lytic efficacy of rt-PA in both clinical and in vitro models. Colucci et al. [118] studied in vitro clot lysis using a radioactive fibrin assay in anticoagulated human clots. They found an average clot lysis of 46% after 3 hours of exposure to rt-PA at a concentration of 0.5 mg/mL. In addition, they found clot lysis of less than 5% in their model for the negative control clots. These findings are corresponding to ours, namely we observed slight thrombus dissolution at the negative control, which we believe was related to a spontaneous break down of the fibrin network. Trusen et al. [119] measured thrombolytic therapy efficiency on either human newborn and or adult whole blood clots focusing on the time dependence of lytic exposure. The progress of clot lysis was determined by estimating the percentage of mass loss of clots before and after lytic assay. Regarding their determination, the clot lysis is only a few percent in rt-PA–treated positive control clots after 30 minutes of exposure, and then they observed increasing dissolution velocity. These observations are consistent with our results. During the first 30 minutes, we found a slow mass dissolution and dissolution rate in case of rt-PA, and then the rt-PA provided two orders of magnitude higher mass dissolution and dissolution rate increase from 30 minutes to 90 minutes. These results suggest that our model is properly designed and it potentially could be used to

understand the effect of iodine concentration on Actilyse. We studied two concentration of iodine in the current paper: 30 mg and 60 mg. These concentrations were chosen based on clinically recommended dosages: fixed dose of contrast medium is to base the contrast media dose on the patient's total body weight. However, this technique can result in an over- or under-dosage of contrast media for some patients. Too little contrast medium may decrease the sensitivity and specificity for detecting lesions in solid organs, particularly the liver, spleen, and pancreas [120]. Too much contrast medium contributes to increase the risk of renal toxicity, which has been proved to be dosing related [121]. Thus, depending on the patient's total body weight either a lower (30 mg) or a higher (60 mg) dose of iodine is infused to obtain an appropriate CT image. We hypothesized that the action of fibrinolytic drug, recombinant tissue plasminogen activator, would be impaired in the presence of contrast agents. Therefore, we studied the impairment in fibrinolysis at low and high concentrations of the most commonly used contrast media. We tested the five most commonly used contrast media, namely Xenetix® (iobitridol), Ultravist® (iopromide), Omnipaque® (iohexol), Visipaque® (iodixanol) and Iomeron® (iomeprol), each in two concentrations: 30 and 60 mg of active substance, iodine. For the study, we used the same experimental set-up for each contrast agents, to highlight their effect on fibrinolysis. We expected the effect to be independent the physical parameters (e.g. osmolality, viscosity) since the chosen contrast media are widely accepted and used in the clinical practice. The results of the present study confirm this hypothesizes. For both 30 mg and 60 mg iodine group, in the first 30 minutes the impairment of clot lysis is not prominent, the clot dissolution rate is imperceptibly lower (~5%) than in case of rt-PA alone (**Fig. 6** and **Fig. 7**). The statistical analyses didn't show significant differences in the solution rates, which means that the contrast media might not considerably affect the rt-PA in the first 30 minutes. However, after 30 minutes there is a major 50% drop in dissolution rate for 30

mg iodine concentration comparing to the only rt-PA treated group. In case of the 60 mg the dissolution rate decrease is stronger, it's approximately 80%. One of possible explanations for failure of clot lysis is that contrast agents alter structure of fibrin, thus, clots became more resistant which leads to a lower efficiency of thrombolytic drugs. Support for this explanation comes from previous studies' in vitro data showing that diatrizoate and iopamidol cause then an alteration in fibrin structure [118,122,123]. This fibrin structure alteration induced by diatrizoate or iohexol was confirmed in vivo using blood samples obtained during the course of cardiac catheterization [123]. Additionally, several studies showed large differences in the radiographic contrast media-induced formation of echinocytes, since the membrane integrity can be compromised by contrasts agents (iopromid, iodixanol) leading to the release of free hemoglobin as an indicator of hemolysis as well [124-126]. However, in this study we did not observe the morphology of red blood cells, thus, we cannot distinguish between contrast agents induced hemolysis and blood clot dissolution by rt-PA. (Note, that we lysed the red blood cells via lysis buffer prior to the spectrophotometry measurement of hemoglobin. Taken together, these results suggest that high levels of iodine really do influence thrombolytic therapy performed by rt-PA. Specifically, our results suggest that when blood clots were exposed with high quantity of iodine, the thrombus dissolution rate dramatically decreased. However, it should be noted that all contrast agents had the same effect, and statistically there was no differences in dissolution rate between Xenetix® (iobitridol), Ultravist® (iopromide), Omnipaque® (iohexol), Visipaque® (iodixanol) and Iomeron® (iomeprol) at 30 or 60 mg of active substance. Low iodine level appeared to decrease less the dissolution rate. However, based on the findings of other studies, contrast agents as such do not impair the action of the drugs; rather, they cause an alteration in fibrin that renders it inherently more resistant to fibrinolysis.

Conclusion

These data demonstrate that radiographic contrast agents impede fibrinolysis. These findings may have clinical relevance when thrombolytic drugs are used at the time of Computed Tomography. This dosage study used an in vitro model to perform thrombus lysis with rt-PA for comparison between the most commonly used iodine-containing contrast agents: Xenetix® (iobitridol), Ultravist® (iopromide), Omnipaque® (iohexol), Visipaque® (iodixanol) and Iomeron® (iomeprol). The experimental results demonstrated that presence of these contrast media negatively affects the efficiency of the fibrinolysis induced by rt-PA. Furthermore, a higher dose of iodine-containing contrast media potentially could further reduce the efficiency of the thrombolytic therapy performed by rt-PA. For future work, we plan to study the effect of iodinated contrast media to thrombolytic therapy by a rat embolic model to confirm these finding in *in vivo* environment.

T-PA Immobilization on Iron Oxide Nanocubes and Localized Magnetic Hyperthermia Accelerate Blood Clot Lysis[116] [1]

Experimental Section

Materials

Cathflo activase (Alteplase) (t-PA) was purchased from Genentech Inc. Bovine thrombin was purchased from Calbiochem. Lipophilic carbocyanine DiD was purchased from Invitrogen. CD41 (Clone MW Reg30) was purchased from BD Pharminogen. 4-biphenylcarboxylic acid (99%) was purchased from Acros Organics. All other chemicals and solvents were purchased from Sigma-Aldrich.

Synthesis of Fe3O4 Magnetic Nanoparticles and Coating with Albumin and t-PA mixture

The synthesis of iron oxide NCs was modified from the reported protocol [127]. Briefly, 2 mmol of iron acetylacetonate and 4.5 mmol of oleic acid were mixed in 10 mL benzyl ether. After degassing at 60 °C for 1 h, the reaction mixture was heated to 200 °C under N2 flow for 2 h with vigorous stirring. Finally, the temperature was increased to 280 °C (20 °C min−1) with reflux system. After cooling to room temperature, the resulting material was centrifuged using acetone/toluene at 6000 rpm for 30 min. The iron oxide nanocubes were purified three times and stored in toluene. The t-PA–NCs nanoparticles were generated by covering the 20 nm nanocubes with a mixture of human tissue plasminogen activator and bovine albumin serum. Briefly, 100 μL of 20 nm nanocubes (0.15 mg in toluene) was mixed with 600 μL BSA (5 mg mL−1 in water) and 100 μg t-PA (human tissue plasminogen activator, 1 mg mL−1 in water). 4 mL of 0.1 m sodium bicarbonate buffer was added to this mixture and probe sonicated for 1–2 min on an ice bath until a homogeneous milky solution

[1] This chapter is based on reference 116: Voros, E., et al., TPA Immobilization on Iron Oxide Nanocubes and Localized Magnetic Hyperthermia Accelerate Blood Clot Lysis. Advanced Functional Materials, 2015. 25(11): p. 1709-1718

was formed. To remove the organic solvent, the solution was stirred with an external magnet overnight.

Recovering t-PA–NCs Nanoparticles: NPs were filtered with a syringe membrane filter (porous 1.0 μm). The solution was then centrifuged using an Amicon Ultra centrifugal filter (Millipore, Billerica, MA) with a molecular-weight cutoff of 10 kDa for 3 min at 3500 rpm. The solution was then washed three times with saline solution to remove all organic solvent. After the centrifugation, the t-PA–NCs were filtered one more time using a syringe membrane filter (porous size 0.45 μm) to remove all clustered NCs and stored in saline at 4 °C.

Characterization of t-PA–NCs

The morphology of the particles was analyzed using transmission (TEM) and scanning electron microscopy (SEM) (ZEISS NEON 40). Nanoparticle suspension was placed on carbon conductive double-sided tape, and dried at room temperature. NPs were coated with platinum layer of 5 nm and then imaged by SEM.

Dynamic Light Scattering (DLS) and Zeta Potential Analysis

All water-soluble iron oxide NCs suspensions were analyzed by DLS and zeta potential to measure average hydrodynamic size and surface charge, respectively, using a ZEN-3600 Zetasizer Nano (Malvern, UK) equipped with a HeNe 633 nm laser. The average hydrodynamic size was calculated from the mean size of the first peak of the number distribution. Standard deviations of hydrodynamic size and zeta potential were obtained from triplet measurements.

Transmission Electron Microscopy (TEM)

The TEM images were obtained using a JEOL 2100 field emission gun TEM operating at 200 kV with a single tilt holder using ultrathin carbon type-A 400 mesh copper grids (Ted Pella Inc.). The

average sizes and size variations were obtained by counting over 1000 particles using Image-Pro Plus 5.0 (Media Cybernetics, Inc., Silver Spring, MD).

Inductively Coupled Plasma Optical Emission Spectroscopy (ICP-OES)

The concentration of iron in the iron oxide NCs suspension was measured by a Perkin Elmer ICP-AES instrument equipped with an auto sampler. A purified NCs solutions was acid digested using HNO3 (70%) and H2O2 (30%) and diluted with deionized water for ICP analysis.

Magnetic Resonance (MR) Relaxivity Measurement

To measure the r1 and r2 relaxivities of individual and clustered iron oxide NCs, a benchtop relaxometer (NMR analyzer, mq 60, Bruker, 1.41T) was used. For each sample, we measured relaxation times T1 and T2 at several iron concentrations [Fe].

Blood Collection and Clotting

Female mice of C57BL/6J background (8–9 months of age) were euthanized via CO2 overdose. Blood was obtained from the inferior vena cava using a 25-gauge needle and 1 mL syringe. 100 μL of blood was then aliquoted into several tubes which contained 50U thrombin solution. The tubes were place at 37 °C for 3 h and then were moved to 4 °C for 3 days ensuring maximal clot retraction, lytic resistance, and stability.

In Vitro Thrombolysis

Thrombolysis without flow was performed by placing the clot in a 7 mL of glass vial, which contained 2.5 mL saline buffer and 200 μg t-PA solution or 200 μL t-PA–NCs solution. The clots were incubated at 37 °C with continuous shaking at 100 rpm for 90 min. The OD415 (optical absorbance) of the supernatant was measured (plate reader) at time point 0, 30, 60, and 90 min post treatment to estimate the amount of released hemoglobin at 415 nm. Thrombolysis with flow was performed by using a micro flow chamber (Parallel Plate Flow Chamber System, Glycotech

Inc.). The flow was fixed at 64.516 μL min−1 with the corresponded shear rate of 10 s−1. A blood clot was placed on a glass plate which was covered with layered collaged type1 to fix the clot on a certain place. Then 1 mL of solution containing the t-PA–NCs or an equivalent volume of free t-PA was injected using a Harvard Apparatus Syringe Pump on the left side of the clot, creating a continuous flow. The lysis was monitored by light microscopy (Inverted EPI Fluorescence microscope by Nikon) and the time required to dissolve the clot was recorded.

Alternating Magnetic Field Experiment

The alternating magnetic field (AMF) was generated at a frequency of 295 KHz and a field amplitude of 42 KA m−1. The mapping of the temperature was monitored using a FLIR A325 infrared camera (FLIR Systems, Inc.). All acquisitions were performed by FLIR ResearchIR Software.

Mouse Ferric Chloride Arterial Injury Model

A previously described model was used with minor modifications [128]. Transgenic Tie2-GFP mice (kind gift from Enrica De Rosa, Houston Methodist Research Institute, Houston, TX) engineered to express GFP in endothelial cells were used in this study. Mice were anesthetized with 2.5%–3% isoflurane and injected with fluorescently labeled red blood cells (RBCs) on the day of imaging in order to allow visualization of blood flow dynamics. Briefly, blood collected retro-orbitally from donor mice was stained with lipophilic carbocyanine DiD (Invitrogen, Carlsbad, CA) at 37 °C using the manufacturer's recommended protocol (1–2 days prior to imaging) and injected (50 μL) retro-orbitally in recipient mice 30 min before imaging. A tail vein catheter was inserted through which a bolus infusion of nanoparticle solution or free t-PA was administered. An incision was made through the abdominal wall to expose the mesentery and arterioles (≈100 μm in diameter) were visualized using an upright Nikon A1R laser scanning confocal microscope and

recorded on Nikon Elements software. After baseline images were acquired, mice were injected retro-orbitally with 30 μL of rat anti-mouse CD41 Clone MW Reg30 (BD Pharminogen) to fluorescently label autologous platelets for the visualization of clot formation. Whatman filter paper saturated with 10% ferric chloride (FeCl3) solution was applied topically for 5 min, which caused denudation of the endothelium and clot formation. 2 to 3 clots per mouse were chosen. 200 μL of saline solution with either NPs loaded with t-PA (100 μg t-PA) or free t-PA (100 μg) were administered through the tail vein catheter 10 min after removal of the ferric chloride filter paper. Following the bolus injection, the vessels were monitored until clot dissolution occurred and lasted for more than 5 s. At the end of the experiment, mice were sacrificed by isoflurane overdose and cervical dislocation. All animal experiments were performed in accordance with protocols reviewed and approved by The Houston Methodist Institutional Animal Care and Use Committee (IACUC).

Statistical Analysis

Values are expressed as mean ± standard error and examined by one-way analysis of variance and Tukey's HSD test. Statistical significance was declared at $P < 0.05$. All the analyses were performed by MINITAB Release 14.13.

Results

Physico-Chemical Characterizations of t-PA–NCs

A schematic representation of t-PA–NCs is shown in **Figure 8a** which depicts two main compartments: a metal core, constituted by multiple 20 nm iron oxide NCs clustered together; a surface layer, obtained by mixing t-PA molecules and bovine serum albumin (BSA). The clustered iron oxide nanocubes are synthesized via high temperature thermal decomposition method, using

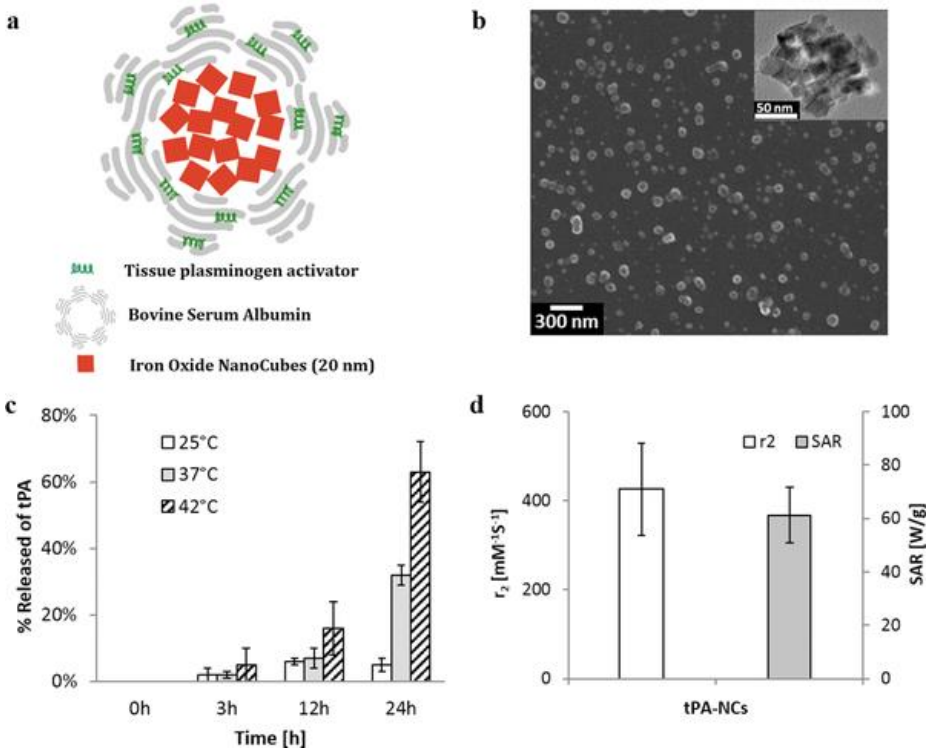

Figure 8: t-PA iron oxide nanocubes (t-PA–NCs). a) Schematic representation of t-PA–NCs showing two main compartments: a cluster of iron oxide nanocubes (NCs) forming the nanoconstruct core; a surface coating of t-PA and serum albumin, forming the external nanoconstruct layer; b) SEM and TEM (inset) images of t-PA–NCs demonstrating a characteristic size of ≈150 nm; c) Release of t-PA from t-PA–NCs at different temperatures (25, 37, and 42 °C) and time points (0, 3, 12, and 24 h); d) Transverse magnetic resonance relaxivity (r_2) (1.41T) and specific absorption rate of t-PA–NCs (f = 512 KHz; H = 10 kA m^{-1}).

iron acetylacetonate as an iron source [129]. The resulting NCs are coated by the t-PA/BSA mixture using an emulsion technique. An electron microscopy analysis of t-PA–NCs reveals nanoconstructs with a quasispherical shape and an average iron core diameter of about 100 nm

(Figure 8b). The transmission electron microscopy image in the inset of **Figure 8b** shows multiple 20 nm iron oxide nanocubes clustered together to form the t-PA–NC core. In aqueous solution, the nanoconstructs show an average hydrodynamic diameter of ≈150 nm. The stability of t-PA–NCs is measured in normal saline solution (0.90% w/v of NaCl) for seven consecutive days. It is observed a moderate reduction in size within the first day followed by a slight increase toward the end of the characterization period. However, the overall variation in hydrodynamic diameter is limited within 10% of the average value. Also, the polydispersity index (PDI) of t-PA–NCs is quite constant over the 7 days characterization returning an average value of 0.20. The surface coating of t-PA–NCs has a slightly negative surface electrostatic charge of about −18 mV which stays constant for the whole observation period. The minor variations in hydrodynamic size, PDI, and surface charge observed over a week would confirm the high stability of t-PA–NCs under physiological conditions. Furthermore, preliminary toxicity analysis performed on murine macrophages has shown negligible effect on cell viability upon incubation with t-PA–NCs.

To gain insights into the loading and release of tissue plasminogen activator from t-PA–NCs, nanoconstructs were synthesized using a green fluorescent labeled t-PA (FITC-t-PA). Thus, by measuring the fluorescent signal associated with t-PA–NCs, the amount of t-PA adsorbed over the nanoconstruct surface was quantified. After generating a calibration curve relating optical absorbance to the number of FITC-t-PA molecules, the total amount of loaded t-PA was estimated to be 0.749 ± 0.08 μg per 9.6 × 1014 nanoconstructs. Following a similar protocol, the release of t-PA molecules was derived at different times points and temperatures. These experiments were performed in 10% serum solution, under mild agitation, and the resulting data are presented in **Figure 8c**. As expected, it is observed that the amount of released t-PA grows with time and temperature. At 3 h post incubation (p.i.), no release is observed at 25 °C, while a ≈2% release is

measured at 37 and 42 °C. At 12 h post incubation, a ≈2% release is detected at 25 °C, which becomes ≈7% and 15% at 37 and 42 °C, respectively. After 24 h of incubation, the percentages of released t-PA are 6%, 32%, and 63%, respectively at 25, 37, and 42 °C. Importantly, within the first few hours, most of the t-PA is still associated with the iron oxide core confirming again the stability of the nanoconstruct surface. Moreover, the release of t-PA at 42 °C tend to be larger than at the physiological temperature suggesting that NC heating could efficiently trigger the local release of t-PA molecules. It is here important to note that t-PA molecules can still activate the fibrinolytic pathway while being immobilized on the nanoconstruct surface. In other words, t-PA does not need to be released in order to form plasmin.The magnetic properties of t-PA–NCs were characterized by quantifying the longitudinal r1 and transverse r2 MR relaxivities, and the specific absorbtion rate (SAR) for magnetic hyperhtermia. The nanoconstructs showed a r2 of ≈450 × 10–3 m−1 s−1 and a SAR of ≈60 W g−1 (**Figure 8d**), which are among the highest values so far reported in the literature for iron oxide nanoconstructs.[18] The iron encapsulation efficiency, defined as the percentage of iron in the t-PA–NCs over the initial input, was of 66% ± 5.6% as measured via ICP-OES.

In Vitro Thrombolytic Efficacy of t-PA–NCs

Two different assays were used for quantifying the t-PA–NC efficacy in dissolving blood clots over time: a static assay, where blood clots were exposed to the thrombolytic agents (free t-PA and t-PA–NCs) in a quiescent fluid; a dynamic assay, where blood clots entrapped within a parallel plate flow chamber were exposed to a flowing solution of thrombolytic agents.

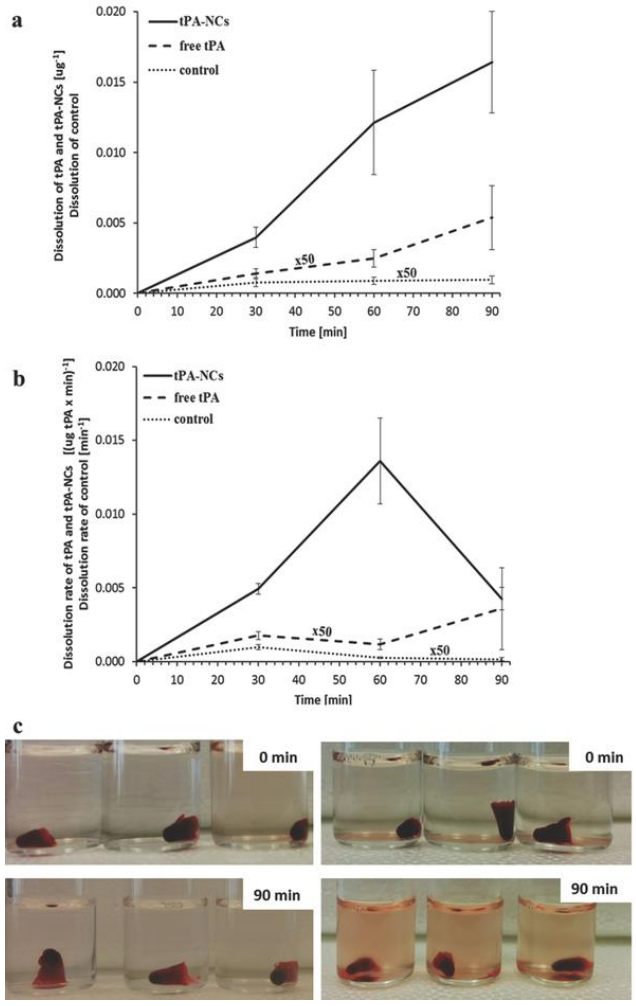

Figure 9: Blood clot dissolution under static conditions. a,b) Dissolution and dissolution rate of blood clots over time exposed to t-PA–NCs, free t-PA, and saline solution (control). Data are normalized by the amounts of t-PA. c) Representative images of blood clots at 0 and 90 min post incubation with saline solution (left) and t-PA–NCs (right).

For the static assay, **Figure 9** show representative images of blood clots at 0 and 90 min, post incubation with thrombolytic agents. Three experimental groups are considered, specifically free t-PA; t-PA–NCs; and control whit clots in a saline solution. The thrombolytic efficacy was quantified by measuring the optical density (OD415) of the supernatant at different time points, namely 0, 30, 60, and 90 min post incubation. The dissolution, which is related to the amount of

lysed clot, and the dissolution rate, which measures the dissolution velocity, are plotted in **Figure 9a,b**, respectively, as a function of time and for the three different experimental groups. As expected, only a minor dissolution of the untreated clot (control) is observed over time, related to a spontaneous break down of the fibrin network. On the other hand, the free drug and t-PA–NCs dissolved the blood clots efficiently (**Figure 9a,b**). In particular, the t-PA nanoconstructs provide two orders of magnitude higher dissolution and dissolution rate as compared to the conventional drug. **Figure 9c** presents representative images of blood clots at different time points, treated with t-PA–NCs or untreated (control). These images clearly show the progressive lysis of the clots treated with t-PA–NCs, where t-PA breaks down the fibrin mesh releasing the red blood cells and inducing a progressive red coloration of the solution.

Next, the thrombolytic efficacy of the t-PA–NCs was assessed in a dynamic assay. In this case, a blood clot was deposited over a microscope glass slide. This slide was assembled in a parallel plate flow chamber apparatus, as schematically shown in **Figure 10a**, eventually mounted on the stage of a microscope. The blood clot was placed in the middle of the chamber deck, partially occluding the flow section. Using a syringe pump, a solution of t-PA–NCs was infused within the parallel plate flow chamber, reaching the blood clot on the left hand side. The blood clot was continuously monitored by light microscopy over a period of 10 min and images of the clot boundaries were taken at different time points (**Figure 10b**). At time 0, the region of interest appeared black for the dense clot. Then, clot lysis started to occur with the infusion of the t-PA–NC solution. At 114 s, the left border of the clot (dashed white line) regressed by ≈1 mm, and even more at 150 s when

the remaining mass of the clot appeared far less dense. The t-PA–NCs solution induced a complete lysis of the clot within the field of view already at 220 s (**Figure 10b**).

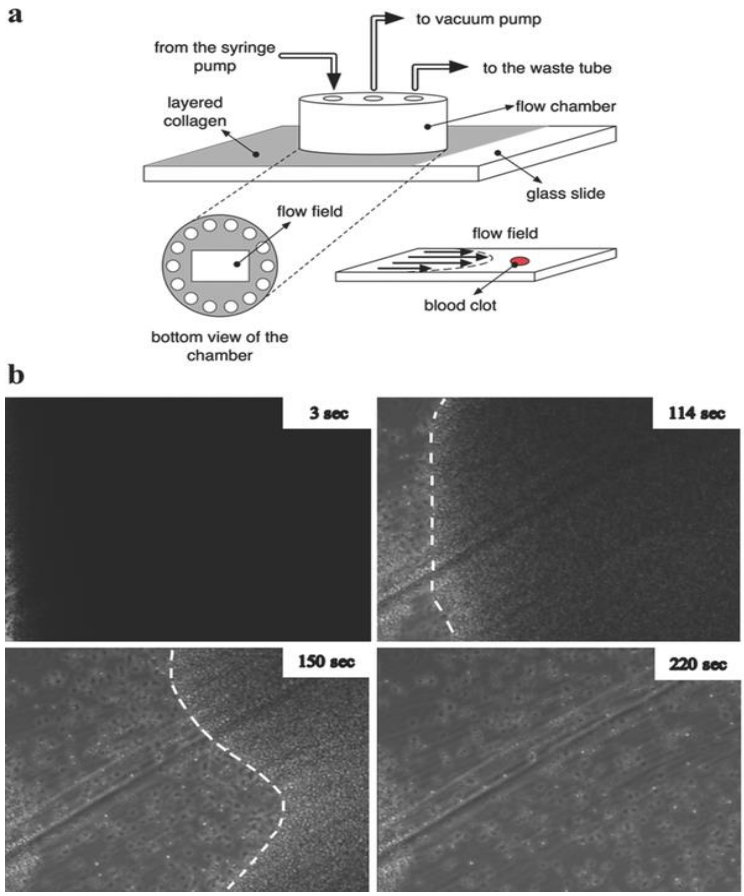

Figure 10: Blood clot dissolution under dynamic conditions. a) Schematic representation of a parallel plate flow chamber system used for reproducing vascular flow. A partially occluding blood clot is deposited in the middle of the chamber over a microscopy glass slide coated with collagen; b) Images of the upstream boundary of a blood clot exposed to a continuous flow of t-PA–NCs. The white dashed line identifies the blood clot upstream boundary while it recedes over time due to progressive dissolution.

Mechano-Chemical Thrombolysis via t-PA–NCs

Upon stimulation with alternating magnetic fields (AMFs), NCs heat up inducing a significantly high local increase in temperature (**Figure 11a,b**). t-PA–NCs have demonstrated a remarkable SAR of ≈60 W g−1, at 512 KHz and 10 kA m−1. Also, the clot busting efficacy of t-PA is known to depend on the temperature and shows a maximum around 45 °C. Following this, NCs and t-PA–NCs were exposed to alternating magnetic fields and temperature maps were captured over time using an infrared camera (**Figure 11a**). In both cases, significant heating is observed within 10 min of exposure to AMF with maximum temperatures of 46.9 ± 1.7 and 49.6 ± 1.3 °C,

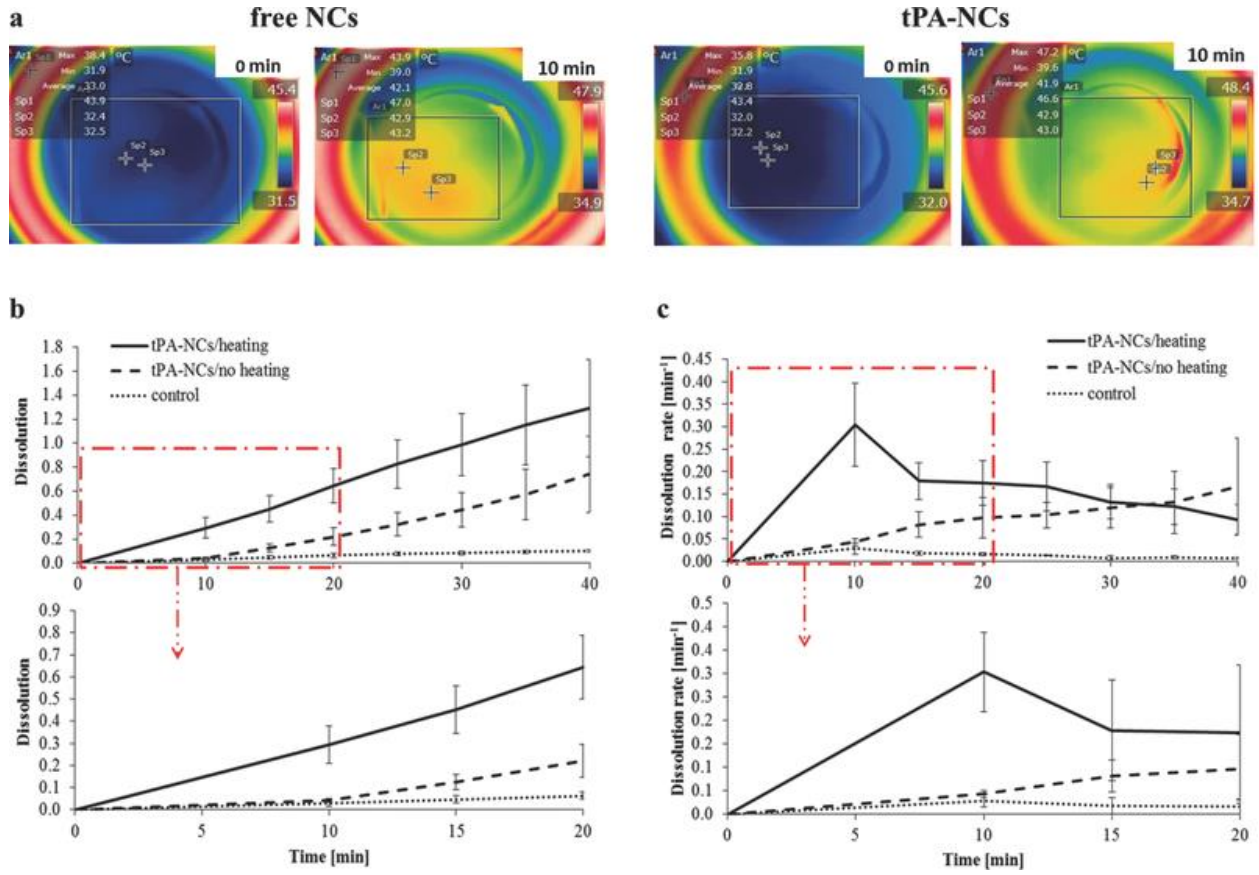

Figure 11: Mechano-chemical lysis of blood clots via magnetic hyperthermia. a) Representative temperature maps of saline solutions in which free NCs and t-PA–NCs are dispersed and exposed to alternating magnetic fields. b,c) Dissolution and dissolution rate of blood clots in the presence of t-PA–NCs either stimulated or not stimulated with alternating magnetic fields. In the control experiments, blood clots were exposed to a saline solution.

respectively, for NCs and t-PA–NCs. Note that the temperature distribution is quite uniform for a saline solution, in the absence of any NCs, and returns a maximum value of about 30 °C. This confirms that the heating is solely specific and is associated with the presence of NCs in solution. Next, the blood clot dissolution and dissolution rates were quantified upon incubation with t-PA–NCs in the presence and absence of AMFs (**Figure 11b,c**). The thrombolytic activity of t-PA–NCs is assessed for a period of 40 min, while exposure to AMF and consequent heating is limited to the first 10 min of incubation. The clot dissolution in the presence of heating was significantly larger than without heating with a time averaged 2-fold increase over the 40 min period (**Figure 11b**). However, a much larger increase can be observed within the first 10 min of incubation (dashed lines in the insets of **Figure 11b,c**), during which NCs are continuously exposed to AMF. These results emphasize the synergy between the chemical and thermo-mechanical effects in clot lysis.

In Vivo Characterization of the Thrombolytic Activity of t-PA–NCs

For determining the in vivo efficacy of the proposed nanoconstructs, intravital micrsocopy (IVM) was used to follow the formation and dissolution of clots over time. [15, 21, 22] Mice were anesthetized with 2.5%–3% isoflurane and injected with 30 μL of rat anti-mouse CD41 Clone MW Reg30 to fluorescently label autologous platelets for the visualization of clot formation and blood flow dynamics. Then, an incision was made through the abdominal wall to expose the mesentery arterioles (≈100 μm in diameter), a Whatman filter paper saturated with 10% ferric chloride ($FeCl_3$) solution was applied topically for 5 min. This caused denudation of the endothelium and clot formation. These steps are documented in **Figure 12a**. After removal of the ferric chloride filter paper; 200 μL of saline solution with either NPs loaded with t-PA (100 μg initial input of t-PA) or soluble t-PA (100 μg) were administered through tail vein. Following the bolus injection,

the vessels were monitored over time (**Figure 12b–d**). Significant differences were observed between the two experimental groups: t-PA–NC injected animals (**Figure 12**) and free t-PA injected animals (**Figure 12d**). Note that 100 μg of initial t-PA input during the t-PA–NC synthesis corresponds to ≈20 μg of actual t-PA immobilized on the NC surface.

In the first case, two clots (Clot 1 and Clot 2) were almost fully occluding a vessel at time 0. The platelets concentration (red signal) between the two clots was minimal documenting the absence of continuous blood flow. Already at 10 s p.i., the structure of the two clots started changing and, at 60 s p.i., the region between Clot 1 and Clot 2 appeared more populated in platelets demonstrating that the vessel was already partially reopened. At 150 s p.i., Clot 1 was almost completely dissolved and the vessel was fully recanalized at 600 s p.i.. Also, the graph of **Figure 12c** shows the actual clot area (A), normalized by the initial value (A0), as a function of time. For the free t-PA case, three clots are identified in the field of view whose areas tend to moderately grow with time rather than decreasing **(Figure 12d,c**). Therefore, at 400 s p.i., the normalized areas of Clot 3, 4, and 5 are larger than the initial values (**Figure 12c**). It should be here recalled that free t-PA has a very short half-life in blood (<5 min in humans, and even shorter in mice), therefore its efficacy can only be seen within the first few minutes post injection.

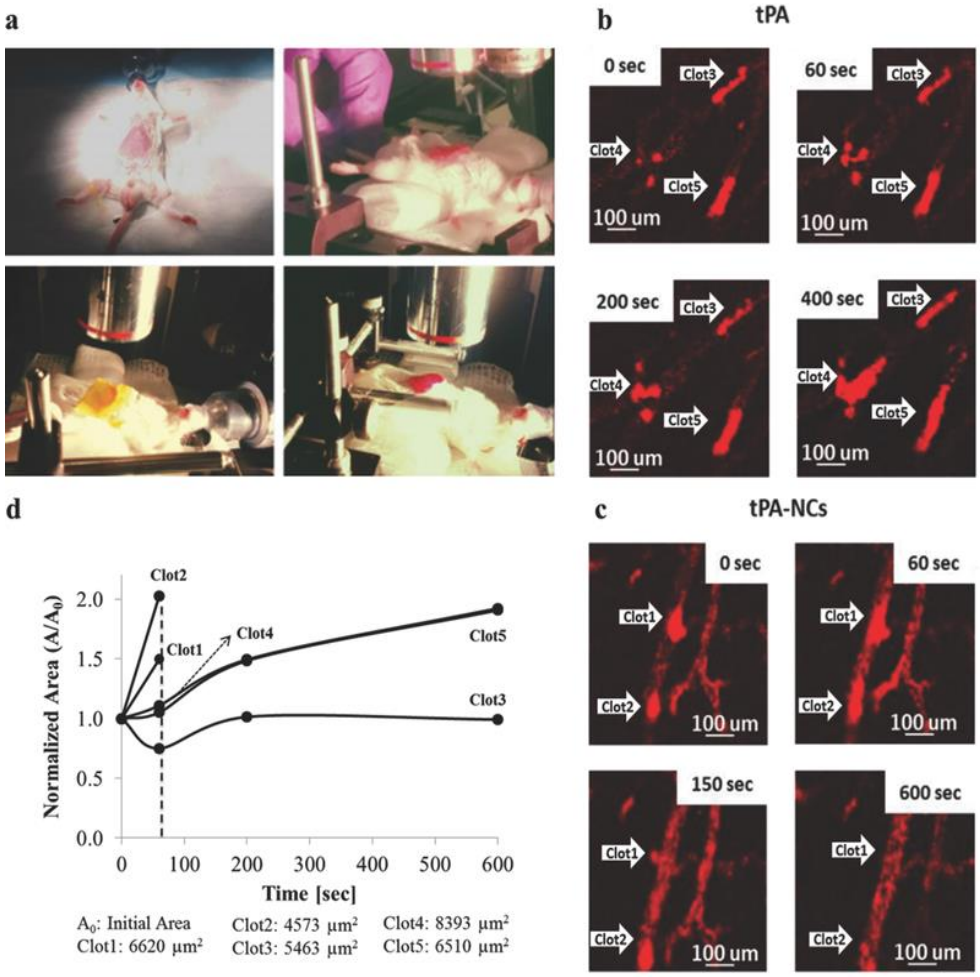

Figure 12. Blood clots in the murine mesentery vasculature monitored in real time via intravital microscopy. a) The endothelium in the mesentery vasculature of a mouse is damaged by a topical treatment with a ferric chloride (FeCl3) solution inducing extensive damage and formation of large, stable blood clots deriving from the intimate mixing of platelets (red dots) and fibrin. b,c) Representative intravital microscopy images of the mesentery vasculature taken at different time points during treatments with free t-PA b) and t-PA–NCs c). Blood clots are identified preinjection and monitored over time up to 10 min post injection of thrombolytic agents. d) Variation with time of the normalized clot area for the five clots identified in the images (b – free t-PA treated mice) and (c – t-PA–NC treated mice). (Injected free t-PA: 5 mg of t-PA/kg of animal; injected t-PA–NCs: ≈1 mg of t-PA/kg animal.)

Discussion and Conclusions

The immobilization of t-PA and serum albumin around a core of iron oxide nanocubes generates thrombolytic nanoconstructs with high stability under physiological conditions and unprecedented efficacy, as compared to free t-PA molecules. t-PA–NCs exhibit a hydrodynamic radius of ≈150 nm, which is preserved up to at least 7 days under physiological conditions. The mixture of t-PA and albumin appears also to control the release of active molecules from the NC surface: only 30% of the initially loaded t-PA is released in the surrounding solution after 24 h (**Figure 9c**), at 37 °C. The release rate is doubled as the local temperature grows to 42 °C, resulting from the exposure of NCs to alternating magnetic fields (AMFs) **(Figure 9d**), whereby over 60% of the loaded dose of t-PA can be released within 24 h. Such a stable association of t-PA to the NC surface is crucial in minimizing the nonspecific release of active agent, particularly in the circulation, and in supporting the direct triggered release of t-PA. Note that t-PA molecules can induced the formation of plasmin in solution even without being released from the NC surface. It is also important to recall that iron oxide nanocubes are biodegradable, as previously shown by these authors and others.[23, 24] Therefore, NCs accumulating nonspecifically within organs of the reticulo-endothelial system, such as the liver and the spleen, would progressively degrade slowly releasing their content, including iron ions that are readily metabolized by cells.[10, 25] Furthermore, complexes of albumin with therapeutic molecules, such as paclitaxel, or imaging agents, such as gadolinium ions, are already approved for clinical use in the treatment of cancer and imaging of cardiovascular diseases.[26-29] Therefore, the building blocks of t-PA–NCs have already demonstrated sufficiently high safety profiles in humans. Indeed, additional studies on t-PA–NCs are needed in order to further advance this system toward clinical trials.

The enhancement in thrombolytic activity of t-PA–NCs over free t-PA demonstrated in vitro and confirmed in vivo should be ascribed to multiple factors. First, the larger size of t-PA–NCs as

compared to free t-PA molecules would support a more intimate mixing of nanoconstructs with the clot matrix. Also, serum albumin is expected to interact with the fibrin network possibly establishing transient bonds that could increase further the permanence of t-PA–NCs within the clot.[30, 31] Moreover, the NC core provides the opportunity of modulating the local temperature amplifying the reaction kinetics in the dissolution process **(Figures 8 and 9**). As demonstrated in **Figure 9**, t-PA–NCs can provide ≈100 times higher dissolution rates compared to free t-PA. In addition to this, exposure to AMF and the consequent localized increase in temperature leads to another 10-fold increase in dissolution rate. In other words, within the same time period, t-PA–NCs would dissolve clots that are 1000 times larger than those treated with free t-PA. Alternatively, a three orders of magnitude lower dose of t-PA would be required to achieve the same clot dissolution effect, thus significantly reducing any side effects.

Furthermore, t-PA–NCs offer potential also in Magnetic Resonance imaging and in remote magnetic guidance, as documented by the authors in previous works.[23, 32] The data of **Figure 8** demonstrate that t-PA–NCs can reach significantly high values of transverse relaxivity r2 equal to about 450 (× 10–3 m s)−1 at 1.41T. This is among the highest r2 values presented in the literature and would suggest that t-PA–NCs can be efficiently used in MR thrombus imaging. This is especially important for cerebral clots whereby MRI can more accurately identify and localize vascular obstructions. Moreover, the unique magnetic properties of NCs can be used for guiding them within the vascular system via external, static magnetic fields. Therefore, the information provided by MR imaging can be used for gathering additional, still circulating t-PA–NCs to the obstructed area using magnetic guidance. This can further enhance the percentage of injected t-PA reaching the biological target and thus reduce the amount of t-PA nonspecifically lost along the circulatory system. Moreover, MR imaging can be used to guide other methods for clot lysis that

could synergistically interact with the mechano-chemical activity of t-PA–NCs. For instance, high intensity focused ultrasound (HIFU) beams could be aimed at the clotted area under the precise guidance of t-PA–NCs and MR imaging.[33, 34]

Our findings demonstrate that a potent, clinically used thrombolytic molecule—tissue plasminogen activator t-PA—can be effectively immobilized on the surface of clustered iron oxide nanocubes to generate a novel nanoconstruct for the dissolution and, potentially, imaging of vascular thrombi. This thrombolytic nanoagent (t-PA–NCs) has demonstrated a three orders of magnitude higher dissolution efficiency as compared to free t-PA and is capable of recanalizing occluded vessels in animal models with sever thrombosis. Also, clustered NCs can be efficient used to vehicle other thrombolytic agents, in addition to t-PA molecules. The intrinsic multifunctional properties of iron oxide nanocubes, which blend together heating, imaging, and remote guidance, and their favorable toxicity profiles make t-PA–NCs a promising platform for the application of nanomedicine in thrombolytic diseases.

6. Conclusion

In our study, first we examined the effect of iodinated contrast media on the efficiency of thrombolysis therapy via recombinant tissue plasminogen activator. We found, that a higher dose of iodinated contrast media might impede fibrinolysis, since the experimental results demonstrated that presence of these contrast media negatively affects the efficiency of the fibrinolysis induced by rt-PA.

Secondly, we examine the preparation of magnetic nanoparticles to use them as a magnetic nanocarrier for delivery of t-PA. MNP consisting of a superparamagnetic core and an bovine serum albumin (BSA) shell was synthesized and characterized. After covalent binding to the MNPs, t-PA showed high activity retention and enhanced storage and operation stability. Effective thrombolysis with MNP-t-PA under magnetic guidance substantially reduced blood clot lysis time compared with runs without magnetic targeting and with free t-PA using the same drug dosage. The results demonstrate that SiO2-MNP is a useful magnetic targeting drug carrier for t-PA delivery, and SiO2-MNP-t-PA may provide a new form of thrombolytic drug that is potentially useful for treatment of thrombus.

In conclusion, t-PA-NCs can be a promising therapeutic agent to improve fibrinolysis, even in those patients who have other injures, thus systematic injection of tissue plasminogen activator could induce life-threating situations, since rt-PA could prevent clog forming at critical locations. Our results can introduce a new concept into the treatment of thrombus, and revolutionize the current medical procedures.

However, the side-effects of the t-PA-NCs requires further investigations, since the reactions of the human immune-system to these nanocarriers is currently unknown.

7. References

1. Mohr JP, Choi DW, Grotta JC, Weir B, Wolf PA. *STROKE—pathophysiology, diagnosis, and management.* 4th ed: Churchill Livingstone, Philadelphia; 2004.
2. Lovlien M, Johansson I, Hole T, Schei B. Early warning signs of an acute myocardial infarction and their influence on symptoms during the acute phase, with comparisons by gender. *Gender medicine.* Sep 2009;6(3):444-453.
3. Segal JB, Eng J, Tamariz LJ, Bass EB. Review of the evidence on diagnosis of deep venous thrombosis and pulmonary embolism. *Annals of family medicine.* Jan-Feb 2007;5(1):63-73.
4. Anderson HV, Willerson JT. Thrombolysis in acute myocardial infarction. *The New England journal of medicine.* Sep 2 1993;329(10):703-709.
5. van der Worp HB, van Gijn J. Clinical practice. Acute ischemic stroke. *The New England journal of medicine.* Aug 9 2007;357(6):572-579.
6. Bennett WF, Paoni NF, Keyt BA, et al. High resolution analysis of functional determinants on human tissue-type plasminogen activator. *The Journal of biological chemistry.* Mar 15 1991;266(8):5191-5201.
7. Robert SD. Preparation of polyethylene glycol-tissue plasminogen activator adducts that retain functional activity: characteristics and behavior in three animal species. *Blood Cells Mol Dis.* 1988(71):1641–1647.
8. Marry TD. Activation of plasminogen by tissue plasminogen activator on normal and thrombasthenic platelets: effects on surface proteins and platelet aggregation. *Blood Cells Mol Dis.* 1986(68):275–280.

9. Kaminski MD, Xie Y, Mertz CJ, Finck MR, Chen H, Rosengart AJ. Encapsulation and release of plasminogen activator from biodegradable magnetic microcarriers. *European journal of pharmaceutical sciences : official journal of the European Federation for Pharmaceutical Sciences.* Sep 2 2008;35(1-2):96-103.

10. Richard KAL. *ACR Manual on Contrast Media.* Vol 10.2: American College of Radiology; 2016.

11. Dillman JR, Ellis JH, Cohan RH, Strouse PJ, Jan SC. Frequency and severity of acute allergic-like reactions to gadolinium-containing iv contrast media in children and adults. *American Journal of Roentgenology.* 2007;189(6):1533-1538.

12. Dillman JR, Ellis JH, Cohan RH, Strouse PJ, Jan SC. Allergic-like breakthrough reactions to gadolinium contrast agents after corticosteroid and antihistamine premedication. *American Journal of Roentgenology.* 2008;190(1):187-190.

13. Goel G, Ravishankar S, Jayakumar P, et al. Intrathecal gadolinium-enhanced magnetic resonance cisternography in cerebrospinal fluid rhinorrhea: road ahead? *Journal of neurotrauma.* 2007;24(10):1570-1575.

14. Brockow K, Romano A, Aberer W, et al. Skin testing in patients with hypersensitivity reactions to iodinated contrast media–a European multicenter study. *Allergy.* 2009;64(2):234-241.

15. Sesé L, Gaouar H, Autegarden JE, et al. Immediate hypersensitivity to iodinated contrast media: diagnostic accuracy of skin tests and intravenous provocation test with low dose. *Clinical & Experimental Allergy.* 2016;46(3):472-478.

16. Mruk B. Renal Safety of Iodinated Contrast Media Depending on Their Osmolarity–Current Outlooks. *Polish Journal of Radiology.* 2016;81:157.

17. Bucher AM, De Cecco CN, Schoepf UJ, et al. Is contrast medium osmolality a causal factor for contrast-induced nephropathy? *BioMed research international.* 2014;2014.

18. Cutroneo P, Polimeni G, Curcuruto R, Calapai G, Caputi AP. Adverse reactions to contrast media: an analysis from spontaneous reporting data. *Pharmacological research.* 2007;56(1):35-41.

19. Bush WH, Swanson DP. Acute reactions to intravascular contrast media: types, risk factors, recognition, and specific treatment. *AJR. American journal of roentgenology.* 1991;157(6):1153-1161.

20. Iakovou I, Zapandiotis A, Mpalaris V, Goulis DG. Radio-contrast agent-induced hyperthyroidism: case report and review of the literature. *Archives of endocrinology and metabolism.* 2016;60(3):287-289.

21. Andreucci M, Solomon R, Tasanarong A. Side effects of radiographic contrast media: pathogenesis, risk factors, and prevention. *BioMed research international.* 2014;2014.

22. Hudzik B, Zubelewicz-Szkodzińska B. Radiocontrast-induced thyroid dysfunction: is it common and what should we do about it? *Clinical endocrinology.* 2014;80(3):322-327.

23. Davis PL. Anaphylactoid reactions to the nonvascular administration of water-soluble iodinated contrast media. *American Journal of Roentgenology.* 2015;204(6):1140-1145.

24. Gaca AM, Frush DP, Hohenhaus SM, et al. Enhancing Pediatric Safety: Using Simulation to Assess Radiology Resident Preparedness for Anaphylaxis from Intravenous Contrast Media 1. *Radiology.* 2007;245(1):236-244.

25. Cohan RH, Ellis JH. Iodinated contrast material in uroradiology: choice of agent and management of complications. *Urologic Clinics of North America.* 1997;24(3):471-491.

26. Cohan RH, Ellis JH, Dunnick NR. Use of low-osmolar agents and premedication to reduce the frequency of adverse reactions to radiographic contrast media: a survey of the Society of Uroradiology. *Radiology.* 1995;194(2):357-364.

27. Marshall Jr G, Lieberman P. Comparison of three pretreatment protocols to prevent anaphylactoid reactions to radiocontrast media. *Annals of allergy.* 1991;67(1):70-74.

28. Barr ML, Chiu HK, Li N, et al. Thyroid Dysfunction in Children Exposed to Iodinated Contrast Media. *The Journal of Clinical Endocrinology & Metabolism.* 2016;101(6):2366-2370.

29. Collen D, Lijnen HR. Molecular basis of fibrinolysis, as relevant for thrombolytic therapy. *Thrombosis and haemostasis.* Jul 1995;74(1):167-171.

30. Cesarman-Maus G, Hajjar KA. Molecular mechanisms of fibrinolysis. *British journal of haematology.* May 2005;129(3):307-321.

31. Cotran RS, Kumar V, Abbas AK, Fausto N, Robbins SL. *Robbins and Cotran pathologic basis of disease.* 7th ed: Philadelphia : Elsevier / Saunders; 2005.

32. Freitas RA, Jr. Nanotechnology, nanomedicine and nanosurgery. *Int J Surg.* 2005;3(4):243-246.

33. Bock A-K, Wagner V, Bärbel Hüsing SG. Nanomedicine Drivers for development and possible impacts *JRC Scientific and Technical reports*2006.

34. Hacke W, Kaste M, Fieschi C, et al. Intravenous thrombolysis with recombinant tissue plasminogen activator for acute hemispheric stroke. The European Cooperative Acute Stroke Study (ECASS). *JAMA : the journal of the American Medical Association.* Oct 4 1995;274(13):1017-1025.

35. Dundar Y, Hill R, Dickson R, Walley T. Comparative efficacy of thrombolytics in acute myocardial infarction: a systematic review. *QJM : monthly journal of the Association of Physicians.* Feb 2003;96(2):103-113.

36. Aspelin P, Stacul F, Thomsen HS, Morcos SK, van der Molen AJ, Members of the Contrast Media Safety Committee of the European Society of Urogenital R. Effects of iodinated contrast media on blood and endothelium. *European radiology.* May 2006;16(5):1041-1049.

37. Dehmer GJ, Gresalfi N, Daly D, Oberhardt B, Tate DA. Impairment of fibrinolysis by streptokinase, urokinase and recombinant tissue-type plasminogen activator in the presence of radiographic contrast agents. *Journal of the American College of Cardiology.* Apr 1995;25(5):1069-1075.

38. Chesebro JH, Knatterud G, Roberts R, et al. Thrombolysis in Myocardial Infarction (TIMI) Trial, Phase I: A comparison between intravenous tissue plasminogen activator and intravenous streptokinase. Clinical findings through hospital discharge. *Circulation.* Jul 1987;76(1):142-154.

39. Heras M, Chesebro JH, Gersh BG, Holmes DR, Mock MB, Fuster V. Emergency thrombolysis in acute myocardial infarction. *Annals of emergency medicine.* Nov 1988;17(11):1168-1175.

40. Dzialowski I, Puetz V, Buchan AM, Demchuk AM, Hill MD, Calgary Stroke P. Does the application of X-ray contrast agents impair the clinical effect of intravenous recombinant tissue-type plasminogen activator in acute ischemic stroke patients? *Stroke.* Jun 2012;43(6):1567-1571.

41. Macdougall NJ, McVerry F, Baird S, Baird T, Teasdale E, Muir KW. Iodinated contrast media and cerebral hemorrhage after intravenous thrombolysis. *Stroke.* March 8 2011 2011;42(8):2170-2174.

42. Yang VC, Naik SS, Song H, Dombkowski AA, Crippen G, Liang JF. Construction and characterization of a t-PA mutant for use in ATTEMPTS: a drug delivery system for achieving targeted thrombolysis. *Journal of controlled release : official journal of the Controlled Release Society.* Dec 10 2005;110(1):164-176.

43. Stief TW, Bunder R, Richter A, Maisch B, Renz H, Fareed J. In vitro simulation of therapeutic plasmatic fibrinolysis. *Clinical and applied thrombosis/hemostasis : official journal of the International Academy of Clinical and Applied Thrombosis/Hemostasis.* Jul 2003;9(3):211-220.

44. Komorowicz E, Kolev K, Lerant I, Machovich R. Flow rate-modulated dissolution of fibrin with clot-embedded and circulating proteases. *Circulation research.* Jun 1 1998;82(10):1102-1108.

45. Basta G, Lupi C, Lazzerini G, Chiarelli P, L'Abbate A, Rovai D. Therapeutic effect of diagnostic ultrasound on enzymatic thrombolysis. An in vitro study on blood of normal subjects and patients with coronary artery disease. *Thrombosis and haemostasis.* Jun 2004;91(6):1078-1083.

46. Beltrami E, Jesty J. Mathematical analysis of activation thresholds in enzyme-catalyzed positive feedbacks: application to the feedbacks of blood coagulation. *Proceedings of the National Academy of Sciences of the United States of America.* Sep 12 1995;92(19):8744-8748.

47. Anand S, Diamond SL. Computer simulation of systemic circulation and clot lysis dynamics during thrombolytic therapy that accounts for inner clot transport and reaction. *Circulation.* Aug 15 1996;94(4):763-774.

48. White LW. Plenty of room at the bottom. *Journal of clinical orthodontics : JCO.* Mar 2001;35(3):127-128.

49. Li X-M, Reinhoudt D, Crego-Calama M. What do we need for a superhydrophobic surface? A review on the recent progress in the preparation of superhydrophobic surfaces. *Chemical Society Reviews.* 2007;36(8):1350-1368.

50. Karn B, Kuiken T, Otto M. Nanotechnology and in situ remediation: a review of the benefits and potential risks. *Environmental Health Perspectives.* 2009;117(12):1813.

51. Pacheco-Torgal F, Jalali S. Nanotechnology: advantages and drawbacks in the field of construction and building materials. *Construction and building materials.* 2011;25(2):582-590.

52. Lu W, Lieber CM. Nanoelectronics from the bottom up. *Nature Materials.* 2007;6(11):841-850.

53. Kroto HW, Heath JR, O'Brien SC, Curl RF, Smalley RE. C 60: buckminsterfullerene. *Nature.* 1985;318(6042):162-163.

54. Testing FIfMRa. Nanotechnologies. *Vocabulary - Part 3: Carbon nano-objects.* Vol ISO/TS 80004-3:20102010.

55. Limbach LK, Wick P, Manser P, Grass RN, Bruinink A, Stark WJ. Exposure of engineered nanoparticles to human lung epithelial cells: influence of chemical composition and catalytic activity on oxidative stress. *Environmental science & technology.* Jun 1 2007;41(11):4158-4163.

56. Nel A, Xia T, Madler L, Li N. Toxic potential of materials at the nanolevel. *Science.* Feb 3 2006;311(5761):622-627.

57. Garnett MC, Kallinteri P. Nanomedicines and nanotoxicology: some physiological principles. *Occup Med (Lond).* Aug 2006;56(5):307-311.

58. Evans MD, Cooke MS. Oxidative damage to DNA in non-malignant disease: biomarker or biohazard? *Genome dynamics.* 2006;1:53-66.

59. Desai TA, Chu WH, Tu JK, Beattie GM, Hayek A, Ferrari M. Microfabricated immunoisolating biocapsules. *Biotechnology and bioengineering.* Jan 5 1998;57(1):118-120.

60. Leoni L, Desai TA. Nanoporous biocapsules for the encapsulation of insulinoma cells: biotransport and biocompatibility considerations. *IEEE transactions on bio-medical engineering.* Nov 2001;48(11):1335-1341.

61. Schinazi RF, Sijbesma R, Srdanov G, Hill CL, Wudl F. Synthesis and virucidal activity of a water-soluble, configurationally stable, derivatized C60 fullerene. *Antimicrobial agents and chemotherapy.* Aug 1993;37(8):1707-1710.

62. Pan X, Redding JE, Wiley PA, Wen L, McConnell JS, Zhang B. Mutagenicity evaluation of metal oxide nanoparticles by the bacterial reverse mutation assay. *Chemosphere.* Mar 2010;79(1):113-116.

63. Liu Y, Xia Q, Liu Y, et al. Genotoxicity assessment of magnetic iron oxide nanoparticles with different particle sizes and surface coatings. *Nanotechnology.* Oct 24 2014;25(42):425101.

64. Fahmy B, Cormier SA. Copper oxide nanoparticles induce oxidative stress and cytotoxicity in airway epithelial cells. *Toxicology in vitro : an international journal published in association with BIBRA.* Oct 2009;23(7):1365-1371.

65. Balasubramanyam A, Sailaja N, Mahboob M, Rahman MF, Hussain SM, Grover P. In vitro mutagenicity assessment of aluminium oxide nanomaterials using the Salmonella/microsome assay. *Toxicology in vitro : an international journal published in association with BIBRA.* Sep 2010;24(6):1871-1876.

66. Balasubramanyam A, Sailaja N, Mahboob M, Rahman MF, Hussain SM, Grover P. In vivo genotoxicity assessment of aluminium oxide nanomaterials in rat peripheral blood cells using the comet assay and micronucleus test. *Mutagenesis.* May 2009;24(3):245-251.

67. Maynard AD, Aitken RJ, Butz T, et al. Safe handling of nanotechnology. *Nature.* Nov 16 2006;444(7117):267-269.

68. Tyner KM, Schiffman SR, Giannelis EP. Nanobiohybrids as delivery vehicles for camptothecin. *Journal of controlled release : official journal of the Controlled Release Society.* Mar 24 2004;95(3):501-514.

69. Hassan MH. Nanotechnology. Small things and big changes in the developing world. *Science.* Jul 1 2005;309(5731):65-66.

70. Son SJ, Reichel J, He B, Schuchman M, Lee SB. Magnetic nanotubes for magnetic-field-assisted bioseparation, biointeraction, and drug delivery. *Journal of the American Chemical Society.* May 25 2005;127(20):7316-7317.

71. Gurzau ES, Neagu C, Gurzau AE. Essential metals--case study on iron. *Ecotoxicology and environmental safety.* Sep 2003;56(1):190-200.

72. Gupta AK, Gupta M. Synthesis and surface engineering of iron oxide nanoparticles for biomedical applications. *Biomaterials.* Jun 2005;26(18):3995-4021.

73. Gonzales-Weimuller M, Zeisberger M, Krishnan KM. Size-dependant heating rates of iron oxide nanoparticles for magnetic fluid hyperthermia. *Journal of magnetism and magnetic materials.* Jul 2009;321(13):1947-1950.

74. Lu AH, Salabas EL, Schuth F. Magnetic nanoparticles: synthesis, protection, functionalization, and application. *Angewandte Chemie.* 2007;46(8):1222-1244.

75. Otsuka H, Nagasaki Y, Kataoka K. PEGylated nanoparticles for biological and pharmaceutical applications. *Advanced drug delivery reviews.* Feb 24 2003;55(3):403-419.

76. Saha S, Golestanian R, Ramaswamy S. Clusters, asters, and collective oscillations in chemotactic colloids. *Physical review. E, Statistical, nonlinear, and soft matter physics.* Jun 2014;89(6):062316.

77. Vaz AM, Serrano-Ruiz D, Laurenti M, Alonso-Cristobal P, Lopez-Cabarcos E, Rubio-Retama J. Synthesis and characterization of biocatalytic gamma-Fe2O3@SiO2 particles as recoverable bioreactors. *Colloids and surfaces. B, Biointerfaces.* Feb 1 2014;114:11-19.

78. Verwey EJ. Theory of the stability of lyophobic colloids. *The Journal of physical and colloid chemistry.* May 1947;51(3):631-636.

79. Laurent S, Forge D, Port M, et al. Magnetic iron oxide nanoparticles: synthesis, stabilization, vectorization, physicochemical characterizations, and biological applications. *Chemical reviews.* Jun 2008;108(6):2064-2110.

80. Tombacz E, Turcu R, Socoliuc V, Vekas L. Magnetic iron oxide nanoparticles: Recent trends in design and synthesis of magnetoresponsive nanosystems. *Biochemical and biophysical research communications.* Dec 18 2015;468(3):442-453.

81. He J, Huang M, Wang D, Zhang Z, Li G. Magnetic separation techniques in sample preparation for biological analysis: a review. *Journal of pharmaceutical and biomedical analysis.* Dec 2014;101:84-101.

82. Moros M, Pelaz B, Lopez-Larrubia P, Garcia-Martin ML, Grazu V, de la Fuente JM. Engineering biofunctional magnetic nanoparticles for biotechnological applications. *Nanoscale.* Sep 2010;2(9):1746-1755.

83. Yang K, Feng L, Shi X, Liu Z. Nano-graphene in biomedicine: theranostic applications. *Chem Soc Rev.* Jan 21 2013;42(2):530-547.

84. Laurent S, Dutz S, Hafeli UO, Mahmoudi M. Magnetic fluid hyperthermia: focus on superparamagnetic iron oxide nanoparticles. *Advances in colloid and interface science.* Aug 10 2011;166(1-2):8-23.

85. Levy M, Wilhelm C, Siaugue JM, Horner O, Bacri JC, Gazeau F. Magnetically induced hyperthermia: size-dependent heating power of gamma-Fe(2)O(3) nanoparticles. *Journal of physics. Condensed matter : an Institute of Physics journal.* May 21 2008;20(20):204133.

86. Kenny GD, Bienemann AS, Tagalakis AD, et al. Multifunctional receptor-targeted nanocomplexes for the delivery of therapeutic nucleic acids to the brain. *Biomaterials.* Dec 2013;34(36):9190-9200.

87. Carrey N. Coasting to DSM-5 - Parental Alienation Syndrome and Child Psychiatric Syndromes: We are what and who we define. *Journal of the Canadian Academy of Child*

and Adolescent Psychiatry = Journal de l'Academie canadienne de psychiatrie de l'enfant et de l'adolescent. Aug 2011;20(3):163.

88. Carrey N. Systemic helter-skelter: are current child psychiatric services missing the boat? *Journal of the Canadian Academy of Child and Adolescent Psychiatry = Journal de l'Academie canadienne de psychiatrie de l'enfant et de l'adolescent.* May 2011;20(2):84-85.

89. Singh N, Jenkins GJ, Asadi R, Doak SH. Potential toxicity of superparamagnetic iron oxide nanoparticles (SPION). *Nano reviews.* 2010;1.

90. Latorre M, Rinaldi C. Applications of magnetic nanoparticles in medicine: magnetic fluid hyperthermia. *Puerto Rico health sciences journal.* Sep 2009;28(3):227-238.

91. McBain SC, Yiu HH, Dobson J. Magnetic nanoparticles for gene and drug delivery. *International journal of nanomedicine.* 2008;3(2):169-180.

92. Bulte JW, Kraitchman DL. Monitoring cell therapy using iron oxide MR contrast agents. *Current pharmaceutical biotechnology.* Dec 2004;5(6):567-584.

93. Burtea C, Laurent S, Mahieu I, et al. In vitro biomedical applications of functionalized iron oxide nanoparticles, including those not related to magnetic properties. *Contrast media & molecular imaging.* Jul-Aug 2011;6(4):236-250.

94. Long NV, Yang Y, Teranishi T, Thi CM, Cao Y, Nogami M. Biomedical Applications of Advanced Multifunctional Magnetic Nanoparticles. *Journal of nanoscience and nanotechnology.* Dec 2015;15(12):10091-10107.

95. Weinstein JS, Varallyay CG, Dosa E, et al. Superparamagnetic iron oxide nanoparticles: diagnostic magnetic resonance imaging and potential therapeutic applications in neurooncology and central nervous system inflammatory pathologies, a review. *Journal*

of cerebral blood flow and metabolism : official journal of the International Society of Cerebral Blood Flow and Metabolism. Jan 2010;30(1):15-35.

96. Medeiros SF, Santos AM, Fessi H, Elaissari A. Stimuli-responsive magnetic particles for biomedical applications. *International journal of pharmaceutics.* Jan 17 2011;403(1-2):139-161.

97. Bulte JW, Kraitchman DL. Iron oxide MR contrast agents for molecular and cellular imaging. *NMR in biomedicine.* Nov 2004;17(7):484-499.

98. Guccione S, Li KC, Bednarski MD. Molecular imaging and therapy directed at the neovasculature in pathologies. How imaging can be incorporated into vascular-targeted delivery systems to generate active therapeutic agents. *IEEE engineering in medicine and biology magazine : the quarterly magazine of the Engineering in Medicine & Biology Society.* Sep-Oct 2004;23(5):50-56.

99. Taylor A, Wilson KM, Murray P, Fernig DG, Levy R. Long-term tracking of cells using inorganic nanoparticles as contrast agents: are we there yet? *Chem Soc Rev.* Apr 7 2012;41(7):2707-2717.

100. Rumenapp C, Gleich B, Haase A. Magnetic nanoparticles in magnetic resonance imaging and diagnostics. *Pharmaceutical research.* May 2012;29(5):1165-1179.

101. Vigor KL, Kyrtatos PG, Minogue S, et al. Nanoparticles functionalized with recombinant single chain Fv antibody fragments (scFv) for the magnetic resonance imaging of cancer cells. *Biomaterials.* Feb 2010;31(6):1307-1315.

102. Mahmoudi M, Sant S, Wang B, Laurent S, Sen T. Superparamagnetic iron oxide nanoparticles (SPIONs): development, surface modification and applications in chemotherapy. *Advanced drug delivery reviews.* Jan-Feb 2011;63(1-2):24-46.

103. Lin MM, Kim DK, El Haj AJ, Dobson J. Development of superparamagnetic iron oxide nanoparticles (SPIONS) for translation to clinical applications. *IEEE transactions on nanobioscience.* Dec 2008;7(4):298-305.

104. Gilchrist RK, Medal R, Shorey WD, Hanselman RC, Parrott JC, Taylor CB. Selective inductive heating of lymph nodes. *Annals of surgery.* Oct 1957;146(4):596-606.

105. Kievit FM, Zhang M. Cancer nanotheranostics: improving imaging and therapy by targeted delivery across biological barriers. *Advanced materials.* Sep 22 2011;23(36):H217-247.

106. Ito A, Honda H, Kobayashi T. Cancer immunotherapy based on intracellular hyperthermia using magnetite nanoparticles: a novel concept of "heat-controlled necrosis" with heat shock protein expression. *Cancer immunology, immunotherapy : CII.* Mar 2006;55(3):320-328.

107. Lu Z, Prouty MD, Guo Z, Golub VO, Kumar CS, Lvov YM. Magnetic switch of permeability for polyelectrolyte microcapsules embedded with Co@Au nanoparticles. *Langmuir : the ACS journal of surfaces and colloids.* Mar 1 2005;21(5):2042-2050.

108. Hamaguchi S, Tohnai I, Ito A, et al. Selective hyperthermia using magnetoliposomes to target cervical lymph node metastasis in a rabbit tongue tumor model. *Cancer science.* Sep 2003;94(9):834-839.

109. Koneracka M, Muckova M, Zavisova V, et al. Encapsulation of anticancer drug and magnetic particles in biodegradable polymer nanospheres. *Journal of physics. Condensed matter : an Institute of Physics journal.* May 21 2008;20(20):204151.

110. Fernandez-Fernandez A, Manchanda R, McGoron AJ. Theranostic applications of nanomaterials in cancer: drug delivery, image-guided therapy, and multifunctional platforms. *Applied biochemistry and biotechnology.* Dec 2011;165(7-8):1628-1651.

111. Melancon MP, Stafford RJ, Li C. Challenges to effective cancer nanotheranostics. *Journal of controlled release : official journal of the Controlled Release Society.* Dec 10 2012;164(2):177-182.

112. Voros E, Deres L, Halmosi R, Varady E, Toth K, Battyani I. Interactions between iodinated contrast media and tissue plasminogen activator: In vitro comparison study. *Clinical hemorheology and microcirculation.* 2017;66(2):167-174.

113. Yu X, Song SK, Chen J, et al. High-resolution MRI characterization of human thrombus using a novel fibrin-targeted paramagnetic nanoparticle contrast agent. *Magnetic resonance in medicine.* Dec 2000;44(6):867-872.

114. Winter PM, Shukla HP, Caruthers SD, et al. Molecular imaging of human thrombus with computed tomography. *Academic radiology.* May 2005;12 Suppl 1:S9-13.

115. Loren M, Garcia Frade LJ, Torrado MC, Navarro JL. Thrombus age and tissue plasminogen activator mediated thrombolysis in rats. *Thrombosis research.* Oct 1 1989;56(1):67-75.

116. Voros E, Cho M, Ramirez M, et al. TPA Immobilization on Iron Oxide Nanocubes and Localized Magnetic Hyperthermia Accelerate Blood Clot Lysis. *Advanced Functional Materials.* 2015;25(11):1709-1718.

117. Krzywinski M, Altman N. Points of view: designing comparative experiments. *Nature methods.* Jun 2014;11(6):597-598.

118. Colucci M, Scopece S, Gelato AV, Dimonte D, Semeraro N. In vitro clot lysis as a potential indicator of thrombus resistance to fibrinolysis--study in healthy subjects and correlation with blood fibrinolytic parameters. *Thrombosis and haemostasis.* Apr 1997;77(4):725-729.

119. Trusen B, Ries M, Zenker M, et al. Whole blood clot lysis in newborns and adults after adding different concentrations of recombinant tissue plasminogen activator (Rt-PA). *Seminars in thrombosis and hemostasis.* 1998;24(6):599-604.

120. Sica GT, Ji H, Ros PR. CT and MR imaging of hepatic metastases. *AJR. American journal of roentgenology.* Mar 2000;174(3):691-698.

121. Gleeson TG, Bulugahapitiya S. Contrast-induced nephropathy. *AJR. American journal of roentgenology.* Dec 2004;183(6):1673-1689.

122. Gabriel DA, Jones MR, Reece NS, Boothroyd E, Bashore T. Platelet and fibrin modification by radiographic contrast media. *Circulation research.* Mar 1991;68(3):881-887.

123. Granger CB, Gabriel DA, Reece NS, et al. Fibrin modification by ionic and nonionic contrast media during cardiac catheterization. *The American journal of cardiology.* Mar 15 1992;69(8):821-823.

124. Gerk U, Kruger A, Franke RP, Jung F. Effect of radiographic contrast media (Iodixanol, Iopromide) on hemolysis. *Clinical hemorheology and microcirculation.* 2014;58(1):171-174.

125. Kaessmeyer S, Sehl J, Khiao In M, et al. Organotypic soft-tissue co-cultures: Morphological changes in microvascular endothelial tubes after incubation with iodinated contrast media. *Clinical hemorheology and microcirculation.* 2016(Preprint):1-12.

126. Song J, Wang X, Xu X, et al. The effects of non-ionic contrast medium on the hemorheology in vitro and in vivo. *Clinical hemorheology and microcirculation.* 2014;58(3):385-393.

127. Dianzani C, Zara GP, Maina G, et al. Drug delivery nanoparticles in skin cancers. *BioMed research international.* 2014;2014.

128. Valetti S, Mura S, Stella B, Couvreur P. Rational design for multifunctional non-liposomal lipid-based nanocarriers for cancer management: theory to practice. *Journal of nanobiotechnology.* 2013;11(1):S6.

129. Lee AY, Peterson EA. Treatment of cancer-associated thrombosis. *Blood.* 2013;122(14):2310-2317.

8. PUBLICATIONS SUPPORTING THE DISSERTATION

2017

1. Eszter Vörös, László Deres, Róbert Halmosi, Edit Váradi, Kálmán Tóth, István Battyáni
   Interactions between iodinated contrast media and tissue plasminogen activator: In vitro comparison study
   CLINICAL HEMORHEOLOGY AND MICROCIRCULATION: 66(2): p. 167-174. (2017.)
   Impact factor: 1.69

2016

2. Eszter Vörös., Cho M., Garami Z., Battyáni I., Decuzzi P., Tóth K.

   T-PA immobilization on iron oxide nanocubes and localized magnetic hyperthermia accelerate blood clot lysis

   ECR 2016 Book of Abstracts - E - Authors' Index. Insights into Imaging, 2016. 7(1): p. 475-525

2015

3. Eszter Vörös, Cho Minjung, Ramirez Maricela, Palange Anna Lisa, De Rosa Enrica, Key Jaehong, Garami Zsolt, Lumsden Alan B, Decuzzi Paolo
   T-PA Immobilization on Iron Oxide Nanocubes and Localized Magnetic Hyperthermia Accelerate Blood Clot Lysis
   ADVANCED FUNCTIONAL MATERIALS**:** (11) pp. 1709-1718. (2015)
   Impact factor: 12.12

4. Eszter Vörös, Minjung Cho, Garami Zsolt, Paulo Decuzzi, Tóth Kálmán, Battyáni István
   Vas oxid alapú nanoparticulomokhoz kötött t-PA és hypertermia kombinációjával végzett célzott thrombus oldás
   In: X. IME Jubileumi Képalakotó Diagnosztikai Továbbképzés és Konferencia. Konferencia helye, ideje: Budapest, Magyarország, 2015.03.26 Budapest: LARIX Kiadó Kft., pp. 72-77.

6. Eszter Vörös, Minjung Cho, Garami Zsolt, Decuzzi Paolo, Tóth Kálmán, Battyáni István
   Vas oxid alapú nanoparticulomokhoz kötött t-PA és hypertermia kombinációjával végzett célzott thrombus oldás
   IME: INTERDISZCIPLINÁRIS MAGYAR EGÉSZSÉGÜGY / INFORMATIKA ÉS MENEDZSMENT AZ EGÉSZSÉGÜGYBEN **14:**(8) pp. 62-66. (2015)

9. PUBLICATIONS NOT RELATED TO THE DISSERTATION

2017

1. Grishma Khanal, Rose-Ann Huynh, Kian Torabian, Hui Xia, Eszter Vörös, Sergey S Shevkoplyas

   Towards bedside washing of stored red blood cells: a prototype of a simple apparatus based on microscale sedimentation in normal gravity

   ***VOX SANGUINIS* 5:** pp. 167-175. (2017)

   Impact factor:2.85

2. Hui Xia, Grishma Khanal, Briony C Strachan, Eszter Vörös, Nathaniel Z Piety, Sean C Gifford, Sergey S Shevkoplyas

   Washing in hypotonic saline reduces the fraction of irreversibly-damaged cells in stored blood: a proof-of-concept study: Hypotonic washing of stored RBCs

   BLOOD TRANSFUSION (2017)

   Impact factor:1.61

2016

3. Eszter Vörös, Nathaniel Z Piety, Sergey S Shevkoplyas
   A Simple Disposable Device for Bedside Washing of Stored Red Blood Cells.
   Konferencia helye, ideje: Orlando, Amerikai Egyesült Államok, 2016.10.22-2016.10.25.
   Wiley-Blackwell Publishing Ltd., 2016. 1 p. (56.) (ISBN:07030-5774)

4. Eszter Vörös, Nathaniel Z Piety, Sergey S Shevkoplyas
   A Simple Disposable Device for Bedside Washing of Stored Red Blood Cells
   Konferencia helye, ideje: Minneapolis, Amerikai Egyesült Államok, 2016.10.05-2016.10.08.
   2016.

2013

4. Eszter Vörös, Horváth A, Sveiczer A

   Length growth patterns in the mitotic cycle of large fission yeast cells

   ACTA MICROBIOLOGICA ET IMMUNOLOGICA HUNGARICA 60: pp. 107-108. (2013)

2012

5. Horváth A, Rácz-Mónus A, Eszter Vörös, Sveiczer Á

   Sejtnövekedési mintázatok vizsgálata a hasadó élesztőben. Cell growth pattern analysis in fission yeast

   MIKOLÓGIAI KÖZLEMÉNYEK-CLUSIANA 51: pp. 44-45. (2012)

2011

6. Horváth A, Rácz-Mónus A, Eszter Vörös, Sveiczer Á

   Cell length growth patterns and size control in fission yeast mutants

   ACTA MICROBIOLOGICA ET IMMUNOLOGICA HUNGARICA 58:(Suppl.) p. 157. (2011)